= [(release in test - spontaneous release) / (maximum release - spontaneous release)] × 100.

Tumor metastasis

EL-4 cells (4×10^5 cells in 0.2 mL) were injected into mice through the tail vein as described previously [44]. On the same day, 600 ng α-GalCer or the same volume of vehicle was injected i.p. The survival time of each mouse was recorded.

Statistic analysis

Statistical analyses were performed with Student's *t*-test. Values of $p<0.05$ were considered significant. Kaplan-Meier survival graphs were constructed and a log rank comparison of the groups was used to calculate the *p* values.

Acknowledgements: We would like to thank Dr. Kronenberg (La Jolla Institute, USA) for permitting use of the α-GalCer/CD1d-tetramer. This work was supported in part by a grant-in-aid for scientific research on priority areas from the Ministry of Education, Culture, Sports, Science and Technology of Japan, and a grant-in-aid for scientific research from the Japan Society for the Promotion of Science.

Conflict of interest: The authors declare no financial or commercial conflict of interest.

References

1 **Bendelac, A., Savage, P. B. and Teyton, L.,** The biology of NKT cells. *Annu. Rev. Immunol.* 2007. **25:** 297–336.

2 **Godfrey, D. I. and Berzins, S. P.,** Control points in NKT-cell development. *Nat. Rev. Immunol.* 2007. **7:** 505–518.

3 **Kronenberg, M.,** Toward an understanding of NKT cell biology: Progress and paradoxes. *Annu. Rev. Immunol.* 2005. **23:** 877–900.

4 **Nocentini, G. and Riccardi, C.,** GITR: A multifaceted regulator of immunity belonging to the tumor necrosis factor receptor superfamily. *Eur. J. Immunol.* 2005. **35:** 1016–1022.

5 **Shevach, E. M. and Stephens, G. L.,** The GITR-GITRL interaction: Co-stimulation or contrasuppression of regulatory activity? *Nat. Rev. Immunol.* 2006. **6:** 613–618.

6 **Ndhlovu, L. C., Takeda, I., Sugamura, K. and Ishii, N.,** Expanding role of T-cell costimulators in regulatory T-cell function: Recent advances in accessory molecules expressed on both regulatory and nonregulatory T cells. *Crit. Rev. Immunol.* 2004. **24:** 251–266.

7 **Watts, T. H.,** TNF/TNFR family members in costimulation of T cell responses. *Annu. Rev. Immunol.* 2005. **23:** 23–68.

8 **Ronchetti, S., Nocentini, G., Riccardi, C. and Pandolfi, P. P.,** Role of GITR in activation response of T lymphocytes. *Blood* 2002. **100:** 350–352.

9 **Tone, M., Tone, Y., Adams, E., Yates, S. F., Frewin, M. R., Cobbold, S. P. and Waldmann, H.,** Mouse glucocorticoid-induced tumor necrosis factor receptor ligand is costimulatory for T cells. *Proc. Natl. Acad. Sci. USA* 2003. **100:** 15059–15064.

10 **Muriglan, S. J., Ramirez-Montagut, T., Alpdogan, O., Van Huystee, T. W., Eng, J. M., Hubbard, V. M., Kochman, A. A. *et al.*,** GITR activation induces an opposite effect on alloreactive CD4(+) and CD8(+) T cells in graft-*versus*-host disease. *J. Exp. Med.* 2004. **200:** 149–157.

11 **Baltz, K. M., Krusch, M., Bringmann, A., Brossart, P., Mayer, F., Kloss, M., Baessler, T. *et al.*,** Cancer immunoediting by GITR (glucocorticoid-induced TNF-related protein) ligand in humans: NK cell/tumor cell interactions. *FASEB J.* 2007. **21:** 2442–2454.

12 **Liu, B., Li, Z., Mahesh, S. P., Pantanelli, S., Hwang, F. S., Siu, W. O. and Nussenblatt, R. B.,** Glucocorticoid-induced tumor necrosis factor receptor negatively regulates activation of human primary natural killer (NK) cells by blocking proliferative signals and increasing NK cell apoptosis. *J. Biol. Chem.* 2008. **283:** 8202–8210.

13 **Hanabuchi, S., Watanabe, N., Wang, Y. H., Ito, T., Shaw, J., Cao, W., Qin, F. X. and Liu, Y. J.,** Human plasmacytoid predendritic cells activate NK cells through glucocorticoid-induced tumor necrosis factor receptor-ligand (GITRL). *Blood* 2006. **107:** 3617–3623.

14 **Grohmann, U., Volpi, C., Fallarino, F., Bozza, S., Bianchi, R., Vacca, C., Orabona, C. *et al.*,** Reverse signaling through GITR ligand enables dexamethasone to activate IDO in allergy. *Nat. Med.* 2007. **13:** 579–586.

15 **Kawano, T., Cui, J., Koezuka, Y., Toura, I., Kaneko, Y., Motoki, K., Ueno, H. *et al.*,** CD1d-restricted and TCR-mediated activation of valpha14 NKT cells by glycosylceramides. *Science* 1997. **278:** 1626–1629.

16 **Hayakawa, Y., Takeda, K., Yagita, H., Van Kaer, L., Saiki, I. and Okumura, K.,** Differential regulation of Th1 and Th2 functions of NKT cells by CD28 and CD40 costimulatory pathways. *J. Immunol.* 2001. **166:** 6012–6018.

17 **Ikarashi, Y., Mikami, R., Bendelac, A., Terme, M., Chaput, N., Terada, M., Tursz, T. *et al.*,** Dendritic cell maturation overrules H-2D-mediated natural killer T (NKT) cell inhibition: Critical role for B7 in CD1d-dependent NKT cell interferon gamma production. *J. Exp. Med.* 2001. **194:** 1179–1186.

18 **Vinay, D. S., Choi, B. K., Bae, J. S., Kim, W. Y., Gebhardt, B. M. and Kwon, B. S.,** CD137-deficient mice have reduced NK/NKT cell numbers and function, are resistant to lipopolysaccharide-induced shock syndromes, and have lower IL-4 responses. *J. Immunol.* 2004. **173:** 4218–4229.

19 **Kaneda, H., Takeda, K., Ota, T., Kaduka, Y., Akiba, H., Ikarashi, Y., Wakasugi, H. *et al.*,** ICOS costimulates invariant NKT cell activation. *Biochem. Biophys. Res. Commun.* 2005. **327:** 201–207.

20 **Marschner, A., Rothenfusser, S., Hornung, V., Prell, D., Krug, A., Kerkmann, M., Wellisch, D. *et al.*,** CpG ODN enhance antigen-specific NKT cell activation *via* plasmacytoid dendritic cells. *Eur. J. Immunol.* 2005. **35:** 2347–2357.

21 **Uldrich, A. P., Crowe, N. Y., Kyparissoudis, K., Pellicci, D. G., Zhan, Y., Lew, A. M., Bouillet, P. *et al.*,** NKT cell stimulation with glycolipid antigen *in vivo*: Costimulation-dependent expansion, Bim-dependent contraction, and hyporesponsiveness to further antigenic challenge. *J. Immunol.* 2005. **175:** 3092–3101.

22 **Zaini, J., Andarini, S., Tahara, M., Saijo, Y., Ishii, N., Kawakami, K., Taniguchi, M. *et al.*,** OX40 ligand expressed by DCs costimulates NKT and $CD4^+$ Th cell antitumor immunity in mice. *J. Clin. Invest.* 2007. **117:** 3330–3338.

23 **Kim, H. J., Kim, H. Y., Kim, B. K., Kim, S. and Chung, D. H.,** Engagement of glucocorticoid-induced TNF receptor costimulates NKT cell activation *in vitro* and *in vivo*. *J. Immunol.* 2006. **176:** 3507–3515.

24 **Godfrey, D. I., MacDonald, H. R., Kronenberg, M., Smyth, M. J. and Van Kaer, L.,** NKT cells: What's in a name. *Nat. Rev. Immunol.* 2004. **4:** 231–237.

25 **Ota, T., Takeda, K., Akiba, H., Hayakawa, Y., Ogasawara, K., Ikarashi, Y., Miyake, S. *et al.***, IFN-gamma-mediated negative feedback regulation of NKT-cell function by CD94/NKG2. *Blood* 2005. **106:** 184–192.

26 **Wilson, M. T., Johansson, C., Olivares-Villagomez, D., Singh, A. K., Stanic, A. K., Wang, C. R., Joyce, S. *et al.***, The response of natural killer T cells to glycolipid antigens is characterized by surface receptor down-modulation and expansion. *Proc. Natl. Acad. Sci. USA* 2003. **100:** 10913–10918.

27 **Shimizu, J., Yamazaki, S., Takahashi, T., Ishida, Y. and Sakaguchi, S.**, Stimulation of CD25(+)CD4(+) regulatory T cells through GITR breaks immunological self-tolerance. *Nat. Immunol.* 2002. **3:** 135–142.

28 **Takeda, I., Ine, S., Killeen, N., Ndhlovu, L. C., Murata, K., Satomi, S., Sugamura, K. and Ishii, N.**, Distinct roles for the OX40-OX40 ligand interaction in regulatory and nonregulatory T cells. *J. Immunol.* 2004. **172:** 3580–3589.

29 **Sugamura, K., Ishii, N. and Weinberg, A. D.**, Therapeutic targeting of the effector T-cell co-stimulatory molecule OX40. *Nat. Rev. Immunol.* 2004. **4:** 420–431.

30 **Stephens, G. L., McHugh, R. S., Whitters, M. J., Young, D. A., Luxenberg, D., Carreno, B. M., Collins, M. and Shevach, E. M.**, Engagement of glucocorticoid-induced TNFR family-related receptor on effector T cells by its ligand mediates resistance to suppression by $CD4^+CD25^+$ T cells. *J. Immunol.* 2004. **173:** 5008–5020.

31 **Valzasina, B., Guiducci, C., Dislich, H., Killeen, N., Weinberg, A. D. and Colombo, M. P.**, Triggering of OX40 (CD134) on $CD4^+CD25^+$ T cells blocks their inhibitory activity: A novel regulatory role for OX40 and its comparison with GITR. *Blood* 2005. **105:** 2845–2851.

32 **Nocentini, G., Bartoli, A., Ronchetti, S., Giunchi, L., Cupelli, A., Delfino, D., Migliorati, G. and Riccardi, C.**, Gene structure and chromosomal assignment of mouse GITR, a member of the tumor necrosis factor/nerve growth factor receptor family. *DNA Cell Biol.* 2000. **19:** 205–217.

33 **Seino, K., Motohashi, S., Fujisawa, T., Nakayama, T. and Taniguchi, M.**, Natural killer T cell-mediated antitumor immune responses and their clinical applications. *Cancer Sci.* 2006. **97:** 807–812.

34 **Hussain, S., Wagner, M., Ly, D. and Delovitch, T. L.**, Role of regulatory invariant CD1d-restricted natural killer T-cells in protection against type 1 diabetes. *Immunol. Res.* 2005. **31:** 177–188.

35 **Turk, M. J., Guevara-Patino, J. A., Rizzuto, G. A., Engelhorn, M. E., Sakaguchi, S. and Houghton, A. N.**, Concomitant tumor immunity to a poorly immunogenic melanoma is prevented by regulatory T cells. *J. Exp. Med.* 2004. **200:** 771–782.

36 **Cohen, A. D., Diab, A., Perales, M. A., Wolchok, J. D., Rizzuto, G., Merghoub, T., Huggins, D. *et al.***, Agonist anti-GITR antibody enhances vaccine-induced CD8(+) T-cell responses and tumor immunity. *Cancer Res.* 2006. **66:** 4904–4912.

37 **Ramirez-Montagut, T., Chow, A., Hirschhorn-Cymerman, D., Terwey, T. H., Kochman, A. A., Lu, S., Miles, R. C. *et al.***, Glucocorticoid-induced TNF receptor family related gene activation overcomes tolerance/ignorance to melanoma differentiation antigens and enhances antitumor immunity. *J. Immunol.* 2006. **176:** 6434–6442.

38 **Calmels, B., Paul, S., Futin, N., Ledoux, C., Stoeckel, F. and Acres, B.**, Bypassing tumor-associated immune suppression with recombinant adenovirus constructs expressing membrane bound or secreted GITR-L. *Cancer Gene Ther.* 2005. **12:** 198–205.

39 **Wang, H. Y., Lee, D. A., Peng, G., Guo, Z., Li, Y., Kiniwa, Y., Shevach, E. M. and Wang, R. F.**, Tumor-specific human $CD4^+$ regulatory T cells and their ligands: Implications for immunotherapy. *Immunity* 2004. **20:** 107–118.

40 **Kohm, A. P., Williams, J. S. and Miller, S. D.**, Cutting edge: Ligation of the glucocorticoid-induced TNF receptor enhances autoreactive $CD4^+$ T cell activation and experimental autoimmune encephalomyelitis. *J. Immunol.* 2004. **172:** 4686–4690.

41 **Ikarashi, Y., Iizuka, A., Koshidaka, Y., Heike, Y., Takaue, Y., Yoshida, M., Kronenberg, M. and Wakasugi, H.**, Phenotypical and functional alterations during the expansion phase of invariant Valpha14 natural killer T (Valpha14i NKT) cells in mice primed with alpha-galactosylceramide. *Immunology* 2005. **116:** 30–37.

42 **Murata, K., Ishii, N., Takano, H., Miura, S., Ndhlovu, L. C., Nose, M., Noda, T. and Sugamura, K.**, Impairment of antigen-presenting cell function in mice lacking expression of OX40 ligand. *J. Exp. Med.* 2000. **191:** 365–374.

43 **Chen, S., Ishii, N., Ine, S., Ikeda, S., Fujimura, T., Ndhlovu, L. C., Soroosh, P. *et al.***, Regulatory T cell-like activity of $Foxp3^+$ adult T cell leukemia cells. *Int. Immunol.* 2006. **18:** 269–277.

44 **Takeda, K., Seki, S., Ogasawara, K., Anzai, R., Hashimoto, W., Sugiura, K., Takahashi, M. *et al.***, Liver $NK1.1^+$ $CD4^+$ alpha beta T cells activated by IL-12 as a major effector in inhibition of experimental tumor metastasis. *J. Immunol.* 1996. **156:** 3366–3373.

Abbreviations: **α-GalCer:** α-galactosylceramide · **GITR:** glucocorticoid-induced TNF receptor · **iNKT cell:** invariant natural killer T cell · **MNC:** mononuclear cells

Full correspondence: Dr. Naoto Ishii, Department of Microbiology and Immunology, Tohoku University Graduate School of Medicine, 2–1 Seiryo-machi, Aoba-ku, Sendai 980–8575, Japan
Fax: +81-22-717-8097
e-mail: ishiin@mail.tains.tohoku.ac.jp

Current addresses: Dr. Lishomwa C. Ndhlovu, Division of Experimental Medicine, Department of Medicine, San Francisco General Hospital, University of California, San Francisco, San Francisco, CA, USA

Received: 20/1/08
Revised: 23/4/08
Accepted: 11/6/08

Immunology
The Journal of cells, molecules, systems and technologies
British Society for immunology

IMMUNOLOGY ORIGINAL ARTICLE

Role of 2B4-mediated signals in the pathogenesis of a murine hepatitis model independent of Fas and Vα14 NKT cells

Hiroshi Furukawa,[1,2] Hiroshi Kitazawa,[1] Izumi Kaneko,[1] Mitsunobu Matsubara,[3] Masato Nose[4] and Masao Ono[1]

[1]*Department of Pathology, Tohoku University Graduate School of Medicine, Sendai,* [2]*Department of Rheumatology, Clinical Research Center for Allergy and Rheumatology, Sagamihara National Hospital, National Hospital Organization, Sagamihara,* [3]*Division of Molecular Medicine, Center for Translational and Advanced Animal Research, Tohoku University Graduate School of Medicine, Sendai, and* [4]*Department of Pathology, Ehime University School of Medicine, Toon, Japan*

doi:10.1111/j.1365-2567.2008.02936.x
Received 17 June 2008; revised 24 July 2008; accepted 25 July 2008.
Correspondence: H. Furukawa, Department of Pathology, Tohoku University Graduate School of Medicine, Seiryo-machi 2-1, Aoba-ku, Sendai-shi, Japan 980-8575.
Email: hfurukawa@mail.tains.tohoku.ac.jp
Senior author: Masao Ono,
email: onomasao@mail.tains.tohoku.ac.jp

Summary

Concanavalin A (Con A)-induced hepatitis is a T-cell-mediated murine experimental model of autoimmune hepatitis. Mice lacking Vα14 NKT cells were found to be less sensitive to this hepatitis and the MRL/Mp-*Fas*$^{lpr/lpr}$ (MRL/lpr; i.e. Fas deficient) mice were also less sensitive. We report herein that MRL/Mp-*Fas*$^{lpr/lpr}$-*Sap*$^{rpl/-}$ (MRL/lpr/rpl) mice lack Vα14 NKT cells and are deficient in the Fas antigen but sensitive to Con A-induced hepatitis. The signaling lymphocytic activation molecule (SLAM)-associated protein (SAP) is an adaptor molecule containing a Src homology 2 (SH2) domain. We previously reported new mutant mice found among MRL/lpr mice and revealed that SAP deficiency led to the regression of autoimmune phenotypes in mutant MRL/lpr/rpl mice. It was also revealed that $CD4^+$ and $CD8^+$ T cells were effector cells and that blockade of 2B4, one of the SLAM family receptors, inhibited the induction of hepatitis in MRL/lpr/rpl mice. These data suggest that signals mediated by molecules other than SAP from 2B4 in T cells played important roles in the induction of hepatitis in MRL/lpr/rpl mice.

Keywords: 2B4; concanavalin A-induced hepatitis; Fas; SAP; SLAM family receptors

Introduction

Signaling lymphocytic activation molecule (SLAM)-associated protein (SAP) is an adaptor molecule containing a Src homology 2 (SH2) domain. SAP is expressed in T and natural killer (NK) cells and binds to the cytoplasmic domains of SLAM family receptors, resulting in the subsequent recruitment of Fyn.[1] The *SAP* gene is located on the X chromosome and is responsible for X-linked lymphoproliferative disease (XLP).[2] Patients with XLP disease are highly susceptible to the Epstein–Barr virus infection and suffer from infectious mononucleosis, malignant lymphoma and hypergammaglobulinaemia or hypogammaglobulinaemia. This SAP-mediated signal is essential for the development of NKT cells (i.e. unconventional CD1d-restricted T cells with invariant Vα14 T-cell receptors).[3] These Vα14 NKT cells recognize glycolipid antigens on CD1d molecules, such as α-galactosylceramide (α-GalCer) derived from a marine sponge or endogenous isoglobotrihexosyl ceramide, and secrete massive amounts of interleukin (IL)-4 and interferon-γ (IFN-γ).[4,5]

Abbreviations: α-GalCer, α-galactosylceramide; Con A, concanavalin A; EAT-2, Ewing's sarcoma-activated transcript-2; ELISA, enzyme-linked immunosorbent assay; ERT, EAT-2-related transducer; FasL, Fas ligand; GOT, glutamate oxalate transaminase; GPT, glutamic pyruvic transaminase; IFN-γ, interferon-γ; IL, interleukin; mAb, monoclonal antibody; NK, natural killer; PBS, phosphate-buffered saline; RT-PCR, reverse transcription-polymerase chain reaction; SAP, SLAM-associated protein; SH2, Src homology 2; SLAM, signaling lymphocytic activation molecule; TNF-α, tumour necrosis factor-α; XLP, X-linked lymphoproliferative disease.

Concanavalin A (Con A)-induced hepatitis is a murine experimental model of autoimmune hepatitis. Systemic injection of the plant lectin causes haemagglutination; activation of lymphocytes; secretion of cytokines such as tumour necrosis factor-α (TNF-α), IL-6, IFN-γ and IL-4; and subsequent hepatocyte injury.[6] Severe combined immunodeficiency mice and athymic mice are less sensitive to Con A-induced hepatitis, indicating that T cells are involved in hepatitis. This phenomenon is also known to be dependent on the Fas–Fas ligand (FasL) axis and Vα14 NKT cells.[7–9] Several studies have reported that molecules involved in Con A-induced hepatitis are P-selectin, LIGHT (homologous to lymphotoxin, exhibits inducible expression and competes with HSV glycoprotein D for herpes virus entry mediator, a receptor expressed by T lymphocytes), osteopontin, IL-4, IFN-γ and CD1d.[8–14]

The Fas antigen is a member of the TNF superfamily and mediates signals that induce apoptotic cell death. The MRL/Mp-*Fas*$^{lpr/lpr}$ (MRL/lpr) strain, in which the *Fas* gene is disrupted by the insertion of a retroposon, is a lupus-prone strain.[15,16] MRL/lpr mice show severe lymphadenopathy and splenomegaly as a result of the abnormal expansion of *lpr* T cells, $CD4^-$ $CD8^-$ $B220^+$ $Thy1{\cdot}2^+$ αβ T cells. We previously reported new mutant mice found among the MRL/lpr mice and revealed that SAP deficiency regresses the autoimmune phenotypes in the mutant mice MRL/Mp-*Fas*$^{lpr/lpr}$-*Sap*$^{rpl/-}$ (MRL/lpr/rpl).[17] It was reported that MRL/lpr mice are less sensitive to Con A-induced hepatitis.[7] Furthermore, SAP-deficient mice were thought to be less sensitive to Con A-induced hepatitis because they lack Vα14 NKT cells.[3] Here, we report that MRL/lpr/rpl mice are sensitive to Con A-induced hepatitis and attempted to shed light on the mechanisms underlying this paradoxical Con A-induced hepatitis in MRL/lpr/rpl mice, which is independent of Fas and Vα14 NKT cells.

Materials and methods

Mice, cells and reagents

MRL mice were bred under specific pathogen-free conditions in Tohoku University. MRL/+ and MRL/lpr mice were purchased from Charles River Japan (Tokyo, Japan). MRL/lpr/rpl mice have previously been described.[17] The MRL/+/rpl mice were generated by crossing the MRL/+ mice with the MRL/lpr/rpl mice and by subsequent intercrossing of the resulting heterozygous F_1 mice. The F_2 mice were genotyped using the following primer sets: 5′-GAGAAGCTCTTACTCGGTA and 5′-CCACTACCAC GAGATATACT with *Kpn*I digestion for *rpl*; and 5′-GTA AATAATTGTGCTTCGTCAG, 5′-TAGAAAGGTGCACG GGTGTG and 5′-CAAATCTAGGCATTAACAGTG for the *lpr* loci. In all animal experiments, we adhered to the Tohoku University guidelines for animal experiments. Hybridoma cells for anti-CD4 (GK1·5) or anti-CD8 (53-6·72) monoclonal antibodies (mAbs) were provided by Tohoku University, Institute of Development, Aging and Cancer, Cell Resource Center for Biomedical Research. Antibody to asialo GM1 and antibody to Con A were purchased from Wako Pure Chemical Industries (Osaka, Japan). α-GalCer was provided by KIRIN brewery (Gunma, Japan). The other mAbs were purchased from BD Bioscience (Franklin Lakes, NJ).

Con A-induced hepatitis

We used five mice per group for all Con A-induced hepatitis experiments. Con A was dissolved in phosphate-buffered saline (PBS) and 200 μl of the solution was injected intravenously into the tail vein of MRL mice. Plasma glutamate oxalate transaminase (GOT) and glutamic pyruvic transaminase (GPT) levels were monitored 12 hr after the injection using a Fuji Drichem 3500v (Fuji film Co., Tokyo, Japan) with slides of GOT/AST-PIII and GPT/ALT-PIII, according to the manufacturer's instructions. $CD4^+$ or $CD8^+$ T cells, or NK cells, were depleted using monoclonal anti-CD4 or anti-CD8 or anti-asialo GM1, respectively, 3, 2 and 1 day before injection of Con A. The depletion efficiency was confirmed in the peripheral blood using a FACSCalbur flow cytometer (BD Bioscience). Serum levels of IL-4 were measured using enzyme-linked immunosorbent assay (ELISA) (BD Bioscience), according to the manufacturer's instructions.

Histological analysis

Autopsy was performed 12 hr after induction of hepatitis in MRL mice by 25 mg/kg of Con A. Organs from mice were fixed in 10% formalin in 0·01 M phosphate buffer (pH 7·2), embedded in paraffin and cut into sections. The sections were stained with hematoxylin and eosin.

Reverse transcription–polymerase chain reaction and vectors

Total RNA was isolated from MRL/+ splenocytes using Trizol (Invitrogen, Carlsbad, CA). cDNA was synthesized from 5 μg of total RNA using Superscript III (Invitrogen), according to the manufacturer's instructions. Reverse transcription–polymerase chain reaction (RT-PCR) was performed using KOD plus DNA polymerase (Toyobo, Osaka, Japan). The PCR products were subcloned into the sequence vector pCR4Blunt (Invitrogen). The sequences of the inserts were confirmed using BigDye Terminator v3.1 and the ABI Prism 3100 sequencer (Applied Biosystems, Foster City, CA). The expression vector pcDNA3·1A was purchased from Invitrogen. The fragments of the murine immunoglobulin G3 (IgG3) Fc region-FLAG and extracellular domains of the

SLAM family receptors (SLAM, 2B4, CD48, Ly9, CD84 and Ly108) were subcloned into pcDNA3·1A to generate the pcDNASLAMFc, pcDNA2B4Fc, pcDNACD48Fc, pcDNALy9Fc, pcDNACD84Fc and pcDNALy108Fc plasmids.

Hydrodynamics-based gene transfer and ELISA for detection of the Fc fusion protein

For *in vivo* gene expression, hydrodynamic injection of plasmids was performed.[14] Plasmids (10 μg) in 4 ml of lactated Ringer solution were rapidly injected into the tail vein of mice. The expression of the Fc fusion protein in the plasma was confirmed by ELISA. ELISA plates (F96 MAXISORP; Nunc, Roskilde, Denmark) were coated with 10 μg/ml of rabbit anti-FLAG (Sigma, St Louis, MO) in carbonate buffer (15 mM Na_2CO_3, 35 mM $NaHCO_3$) and blocked with 5% skim milk in PBS. After plasma samples were loaded, the fusion protein levels were detected with horseradish peroxidase-labelled rabbit anti-mouse IgG3 (1:5000 dilution; Rockland Immunochemicals, Gilbertsville, PA) and 3,3′,5,5′-tetramethylbenzidine peroxidase substrate (Moss, Inc., Pasadena, MD).

Flow cytometric analysis

Hepatic mononuclear cells were isolated as previously described.[18] Briefly, the liver was pressed through a 70-μm cell strainer (BD Bioscience). Hepatocytes were pelleted by centrifugation at 30 *g* for 3 min. The remaining liver cells in the supernatant were pelleted at 300 *g* for 5 min and then resuspended in a 40% isotonic Percoll solution (GE Healthcare Bioscience, Uppsala, Sweden). The suspension was underlaid with a 60% isotonic Percoll solution. After centrifugation at 1500 *g* for 20 min, mononuclear cells were isolated at the interface. The cells were stained with murine CD1d:Ig (BD Bioscience)-α-GalCer, according to the manufacturer's instructions, and analyzed using a FACSCalibur flow cytometer (BD Bioscience).

Results

MRL/lpr/rpl mice are more susceptible to Con A-induced hepatitis than MRL/lpr mice.

When 21 mg/kg of Con A was intravenously injected into MRL/+ mice, severe hepatitis was induced (Fig. 1a and c); the extent of hepatitis was evaluated by measuring the activities of the two deviation enzymes GOT and GPT and the survival rate. As reported previously,[7] MRL/lpr mice were less sensitive to Con A-induced hepatitis than MRL/+ mice (Fig. 1a,c). However, severe hepatitis was induced in MRL/+ and MRL/lpr/rpl mice when 27 mg/kg of Con A was injected (Fig. 1b,d). These findings were also confirmed by histological analysis. Severe zonal necrosis of hepatocytes was observed in the livers of MRL/+ and MRL/lpr/rpl mice but not in the livers of MRL/lpr mice (Fig. 2). These histological data correlated

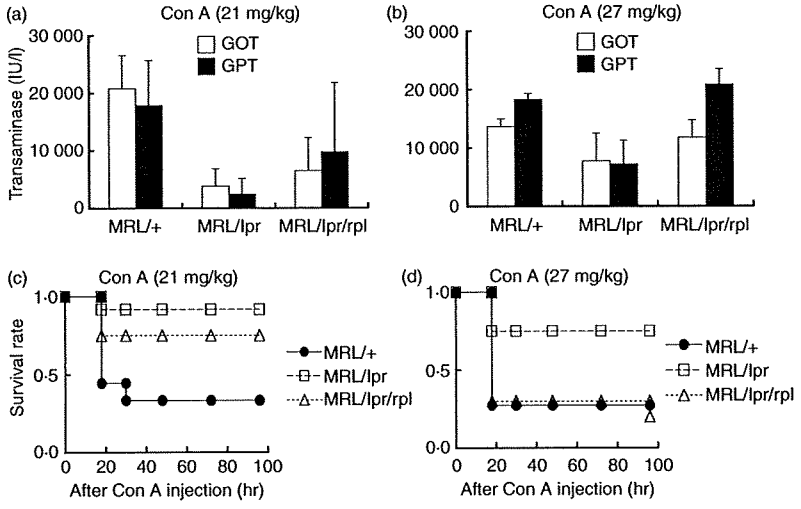

Figure 1. MRL/lpr/rpl mice are susceptible to concanavalin A (Con A)-induced hepatitis. MRL/+, MRL/lpr and MRL/lpr/rpl mice were injected with the indicated dose of Con A into the tail vein. Plasma transaminase levels were measured 12 hr after injection (a,b). Data are presented as mean + standard deviation (SD). MRL mice were injected with the indicated dose of Con A and their survival was monitored thereafter (c,d). GOT, glutamate oxalate transaminase; GPT, glutamic pyruvic transaminase.

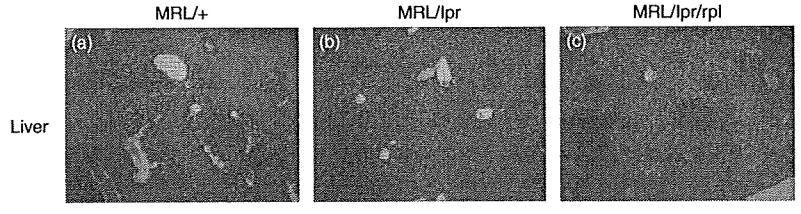

Figure 2. Histological analysis of the liver of MRL mice with induced hepatitis. Microscopic images of the livers of MRL/+ (a), MRL/lpr (b) and MRL/lpr/rpl (c) concanavalin A (Con A)-injected mice after haematoxylin and eosin staining.

with that from the transaminase and survival experiments. Thus, MRL/lpr/rpl mice are susceptible to Con A-induced hepatitis in a Fas-independent manner.

MRL/+/rpl mice are less sensitive to hepatitis

It was of interest to establish whether MRL/+/rpl mice are also susceptible to Con A-induced hepatitis. When 21 mg/kg of Con A was injected, severe hepatitis was induced in MRL/+ mice, but not in MRL/+/rpl mice (Fig. 3a,b). When 27 mg/kg of Con A was injected, severe hepatitis was also induced in MRL/+ mice. However, MRL/+/rpl mice were less sensitive than MRL/+ mice (Fig. 3c). Taken together, the results indicate that MRL/+/rpl mice were less sensitive to Con A-induced hepatitis, and this result was contrary to our expectations.

$CD4^+$ and $CD8^+$ T cells are responsible for the induction of hepatitis in MRL/lpr/rpl mice

We evaluated the role of $CD4^+$ and $CD8^+$ T and NK cells from MRL/+ mice in the induction of hepatitis in MRL/lpr/rpl mice. In MRL/+ mice, treatment with monoclonal anti-CD4 and anti-CD8 abrogated the induction of hepatitis caused by 21 mg/kg of Con A (Fig. 4a,b). Meanwhile, treatment with monoclonal anti-CD4 and anti-CD8 had only a slight effect on the induction of hepatitis in MRL/+ mice caused by 27 mg/kg of Con A (Fig. 4c). Interestingly, treatment of MRL/lpr mice with monoclonal anti-CD8 worsened the prognosis of hepatitis (Fig. 4d), suggesting the involvement of $CD8^+$ T cells in protection against hepatitis. In MRL/lpr/rpl mice, treatment with monoclonal anti-CD4 and anti-CD8 abrogated the induction of hepatitis caused by 27 mg/kg of Con A (Fig. 4e). Treatment with anti-asialo GM1 partially changed the susceptibility of MRL/lpr/rpl mice to hepatitis. Thus, the antibody-depletion study aided in the identification of effector cells in hepatitis induced in MRL/lpr/rpl mice.

Vα14 NKT cells were absent in MRL/lpr/rpl mice

It has been reported that Vα14 NKT cells are absent in SAP-deficient mice.[3] Because MRL/lpr/rpl mice are susceptible to hepatitis and Vα14 NKT cells are essential for the Con A-induced hepatitis, it was hypothesized that Vα14 NKT cells exist in MRL/lpr/rpl mice. It was suggested that Vα14 NKT precursor cells would be depleted in the absence of SAP-mediated signals in a Fas-dependent manner. Flow cytometric analysis of the hepatic mononuclear cells and splenocytes was performed to elucidate the existence of Vα14 NKT cells in MRL/lpr/rpl mice. Vα14 NKT cell numbers in MRL/lpr mice were reduced as reported previously,[19] and contrary to our expectations, Vα14 NKT cells did not exist in the liver or spleen of MRL/lpr/rpl mice (Fig. 5).

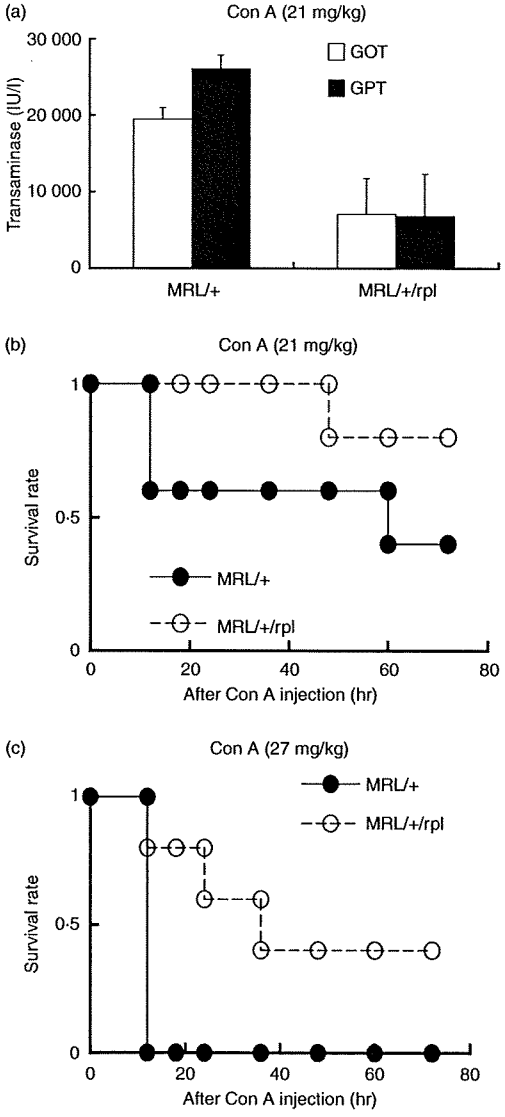

Figure 3. MRL/+/rpl mice are less sensitive to concanavalin A (Con A)-induced hepatitis. MRL/+ and MRL/+/rpl mice were injected with the indicated dose of Con A in the tail vein. Plasma transaminase levels were measured 12 hr after injection (a). Data are presented as mean + standard deviation (SD). MRL mice were injected with the indicated dose of Con A and the subsequent survival was monitored (b,c). GOT, glutamate oxalate transaminase; GPT, glutamic pyruvic transaminase.

IL-4 expression was not observed in hepatitis in MRL/lpr/rpl mice

The expression levels of IL-4 in Con A-induced hepatitis were analyzed. The levels of IL-4 were elevated in sera from MRL/+ mice but not in sera from MRL/lpr or MRL/lpr/rpl

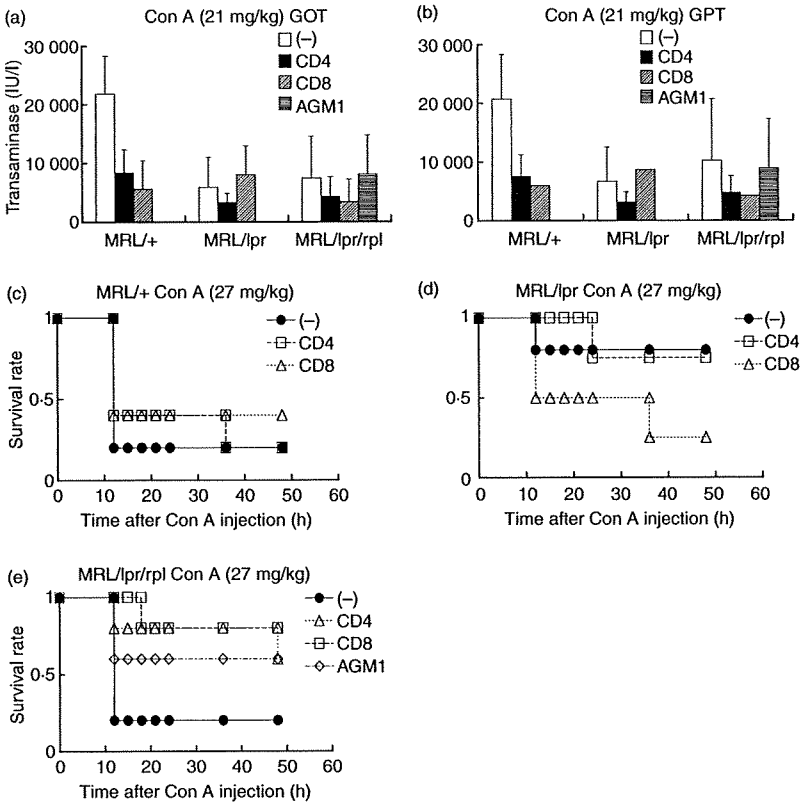

Figure 4. The development of hepatitis in MRL/lpr/rpl mice was mediated by $CD4^+$ and $CD8^+$ T cells. MRL/+, MRL/lpr and MRL/lpr/rpl mice were pretreated with monoclonal anti-CD4 (GK1·5) or anti-CD8 (53–6·72) or anti-asialo GM1 (AGM1) at 3, 2 and 1 day before injection with the indicated dose of concanavalin A (Con A) into the tail vein. Plasma transaminase levels were measured 12 hr after injection of Con A (a,b). Data are presented as mean + standard deviation (SD). MRL mice pretreated with the same antibodies were injected with the indicated dose of Con A and the subsequent survival was monitored (c–e). GOT, glutamate oxalate transaminase; GPT, glutamic pyruvic transaminase.

(Fig. 6a,b). The elevation of IL-4 correlated with the existence of Vα14 NKT cells but not with the induction of hepatitis, suggesting that IL-4 expression is not essential for the induction of hepatitis in MRL/lpr/rpl mice.

The 2B4 molecule is involved in hepatitis in MRL/lpr/rpl mice

To elucidate the role of the SLAM family receptor-mediated signals in MRL/lpr/rpl mice, hydrodynamic injection of plasmids was performed before the induction of hepatitis with 27 mg/kg of Con A (Fig. 7b). In the hepatitis model induced by the injection of 27 mg/kg of Con A, blockade of the 2B4–Fc fusion protein resulted in a significant decrease in plasma transaminase. On the contrary, blockade of the 2B4–Fc fusion protein in MRL/+ mice did not result in a significant decrease in plasma transaminase. In MRL/+ mice expressing CD84–Fc and SLAM–Fc fusion proteins, the GPT level was lower than in the other groups, but the GOT level was comparable (Fig. 7a). The

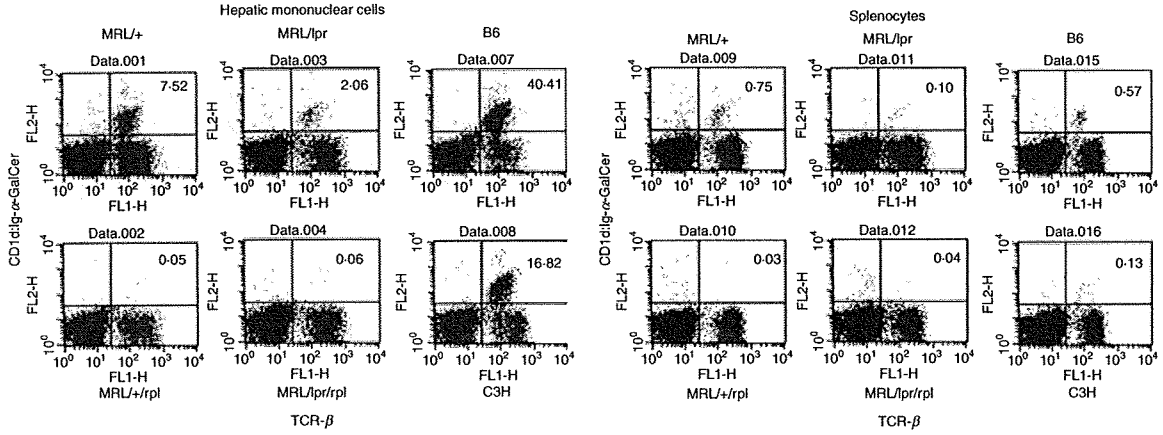

Figure 5. Vα14 NKT cells are absent in MRL/lpr/rpl mice. Hepatic mononuclear cells and splenocytes from MRL mice were stained with murine CD1d:Ig-α-galactosylceramide and monoclonal anti-T-cell receptor (TCR)β chain, and analyzed using a flow cytometer.

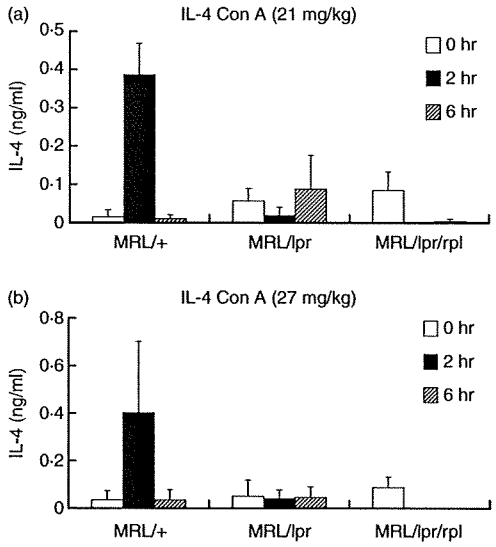

Figure 6. Hepatitis in MRL/lpr/rpl mice was not mediated by interleukin-4 (IL-4). MRL/+, MRL/lpr and MRL/lpr/rpl mice were injected in the tail vein with the indicated dose of concanavalin A (Con A). Serum IL-4 (a,b) levels were measured 0, 2 and 6 hr after injection. Data are presented as mean + standard deviation (SD).

expression of Fc fusion protein in the plasma of treated mice was confirmed in both MRL/+ and MRL/lpr/rpl mice (Fig. 7c). These data suggest that some lymphocyte populations expressing 2B4 are responsible for the induction of hepatitis in MRL/lpr/rpl mice.

Discussion

It is known that mice which lack Vα14 NKT cells and Fas-deficient mice are less sensitive to hepatitis.[7,9] However, in this study, we showed that MRL/lpr/rpl mice which lack Vα14 NKT cells and are deficient for the Fas antigen are sensitive to Con A-induced hepatitis. The hepatitis induced in MRL/lpr/rpl mice was Fas independent. One explanation for this phenomenon is that intravenously injected Con A was expended by the expanded population of lymphocytes, namely $CD4^-$ $CD8^-$ *lpr* T cells, in MRL/lpr mice, thus altering the susceptibility of the MRL/lpr mice. Because the number of *lpr* T cells was reduced in MRL/lpr/rpl mice,[17] these mice were susceptible to hepatitis. However, MRL/lpr mice treated with monoclonal anti-CD8 became susceptible to the hepatitis, even though the splenomegaly and lymphadenopathy were maintained in MRL/lpr mice after treatment with the monoclonal anti-CD8 (Fig. 4d). This finding is not consistent with the Con A-expending hypothesis. The next explanation is that Fas deficiency in the *lpr* mutant is leaky,[7,15] and Fas expressed at low levels mediates the apoptotic signals in hepatocytes of MRL/lpr/rpl mice. The expression of Fas was not detected in MRL/lpr mice or in MRL/lpr/rpl mice.[17] It was reported that the expression of Fas was induced in MRL/lpr mice by the administration of Con A.[7] Although expression of Fas was also induced in MRL/lpr/rpl mice, but not in MRL/lpr mice, the expression levels in MRL/lpr/rpl mice were comparable or relatively lower (expression levels of *Fas* from gene chip data of the spleen before and 3 hr after injection of

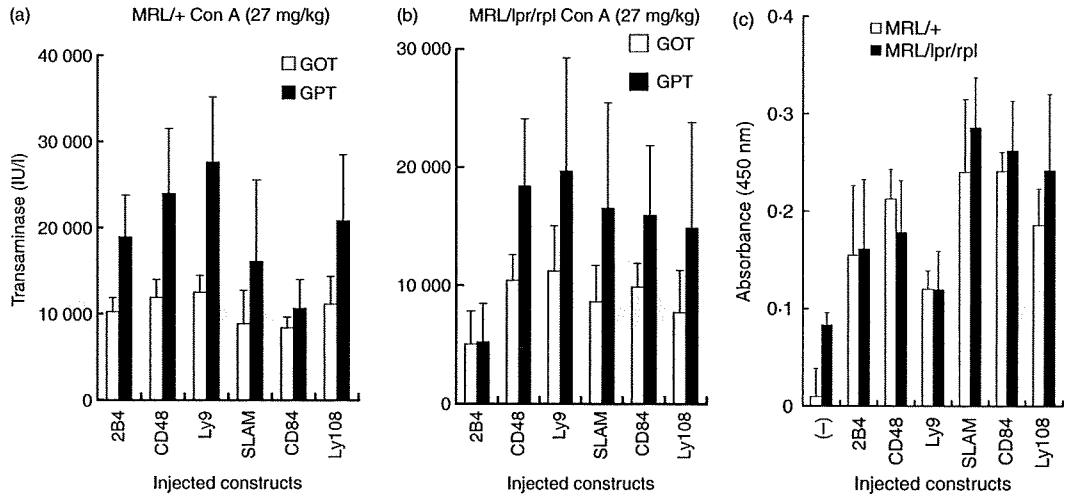

Figure 7. Hepatitis in MRL/lpr/rpl mice was mediated by $2B4^+$ T cells. MRL/+ and MRL/lpr/rpl mice were pretreated by hydrodynamic injection of the indicated plasmids and injected with the indicated dose of concanavalin A (Con A) into the tail vein 10 hr after injection with the plasmid. Plasma transaminase levels were measured 12 hr after injection with Con A (a,b). The expression of the Fc fusion protein in the plasma was confirmed by enzyme-linked immunosorbent assay (ELISA) (c). Data are presented as mean + standard deviation (SD). GOT, glutamate oxalate transaminase; GPT, glutamic pyruvic transaminase.

27 mg/kg of Con A: MRL/lpr: 187·2, 87·9; MRL/lpr/rpl: 25·2, 44·0). Therefore, this hypothesis cannot explain the difference in the susceptibility of the MRL/lpr and MRL/lpr/rpl strains. The other explanation is that the defects in Fas and SAP in MRL/lpr/rpl mice altered the development of some subpopulations of T cells and such newly developed lymphocytes caused the hepatitis instead of the Vα14 NKT cells. It has been reported that SAP deficiency causes a developmental defect in Vα14 NKT cells,[3] but it also causes a developmental defect in another subpopulation of T cells in a Fas-dependent manner. As treatment with monoclonal anti-CD4 and anti-CD8 abrogated the induction of hepatitis in MRL/lpr/rpl mice, and the blockade of 2B4 inhibited the induction of hepatitis in MRL/lpr/rpl mice (Fig. 7), 2B4 but not SAP-mediated signals in $2B4^+$ $CD4^+$ and $2B4^+$ $CD8^+$ T cells played important roles in the induction of the hepatitis in MRL/lpr/rpl mice. As a next step, we should identify which of the $2B4^+$ T-cell subpopulation was responsible for the induction of hepatitis.

The signals from 2B4 molecules were mediated in NK cells by SAP and SAP-related adaptors, Ewing's sarcoma-activated transcript-2 (EAT-2) and EAT-2-related transducer (ERT).[20] EAT-2 and ERT are known to mediate inhibitory signals in NK cells. It is still ambiguous whether the other SAP-related adaptor could be involved in transduction of the activating signals mediated from 2B4 in T cells in the hepatitis induced in MRL/lpr/rpl mice by Con A, even though the possibility of the presence of the other SAP-related adaptors has been raised.[21] The other SAP-related adaptor that can bind to 2B4 would transduce enhanced activating signals in the absence of SAP. However, the transducer of the 2B4-mediated signals in the hepatitis induced in MRL/lpr/rpl mice by Con A is still unknown and should be investigated further.

Vα14 NKT cells are known to be essential for the induction of hepatitis. As Vα14 NKT cells were absent in MRL/lpr/rpl mice (Fig. 5), the Con A-induced hepatitis in MRL/lpr/rpl mice was independent of Vα14 NKT cells. Instead of Vα14 NKT cells, MR-1-restricted Vα19 T cells, recently described as unconventional NKT cells,[22] were candidate $2B4^+$ T cells responsible for hepatitis induction. As the expansion of Vα19 NKT cells in Vα14 NKT-cell-deficient mice has been reported,[23] the number of Vα19 NKT cells could increase in Vα14 NKT-cell-deficient MRL/lpr/rpl mice. Future studies should be carried out to clarify whether this population is expanded in MRL/lpr/rpl mice and if it is responsible for the induction of hepatitis by Con A. It was also reported that expression of IL-4 was caused by Vα14 NKT cells and is essential for induction of the hepatitis.[11] In this study, IL-4 expression was not observed in the MRL/lpr/rpl mice with Con A-induced hepatitis (Fig. 6). This defect in IL-4 expression was a result of the absence of Vα14 NKT cells. Therefore, it is indicated that $2B4^+$ T cells cause hepatitis in MRL/lpr/rpl mice in an IL-4-independent manner. Taken together, the hepatitis induced in MRL/lpr/rpl mice was found to be independent of Fas, Vα14 NKT cells and IL-4, but dependent on signals mediated by adaptors other than SAP from 2B4 in T cells.

Acknowledgements

α-GalCer was provided by KIRIN brewery. We thank Dr Hiroyuki Nishimura (Wakayama Medical University) for fruitful discussions; Ms Fumiko Date, Ms Naoko Shibata and Ms Naomi Yamaki (Tohoku University) for providing technical assistance; and Ms Noriko Fujisawa and Ms Emi Yura (Tohoku University) for secretarial assistance. This study was supported by Grants-in-Aid for Scientific Research from the Ministry of Education, Science, Sports, and Culture of Japan to H.F. (#16790221) and M.O. (#16390113, 19390108 and 19659096).

References

1 Engel P, Eck MJ, Terhorst C. The SAP and SLAM families in immune responses and X-linked lymphoproliferative disease. *Nat Rev Immunol* 2003; **3**:813–21.

2 Sayos J, Wu C, Morra M *et al.* The X-linked lymphoproliferative-disease gene product SAP regulates signals induced through the co-receptor SLAM. *Nature* 1998; **395**:462–9.

3 Nichols KE, Hom J, Gong SY *et al.* Regulation of NKT cell development by SAP, the protein defective in XLP. *Nat Med* 2005; **11**:340–5.

4 Matsuda JL, Gapin L. Developmental program of mouse Valpha14i NKT cells. *Curr Opin Immunol* 2005; **17**:122–30.

5 Yu KO, Porcelli SA. The diverse functions of CD1d-restricted NKT cells and their potential for immunotherapy. *Immunol Lett* 2005; **100**:42–55.

6 Tiegs G, Hentschel J, Wendel A. A T cell-dependent experimental liver injury in mice inducible by concanavalin A. *J Clin Invest* 1992; **90**:196–203.

7 Tagawa Y, Kakuta S, Iwakura Y. Involvement of Fas/Fas ligand system-mediated apoptosis in the development of concanavalin A-induced hepatitis. *Eur J Immunol* 1998; **28**:4105–13.

8 Kaneko Y, Harada M, Kawano T, Yamashita M, Shibata Y, Gejyo F, Nakayama T, Taniguchi M. Augmentation of Valpha14 NKT cell-mediated cytotoxicity by interleukin 4 in an autocrine mechanism resulting in the development of concanavalin A-induced hepatitis. *J Exp Med* 2000; **191**:105–14.

9 Takeda K, Hayakawa Y, Van Kaer L, Matsuda H, Yagita H, Okumura K. Critical contribution of liver natural killer T cells to a murine model of hepatitis. *Proc Natl Acad Sci U S A* 2000; **97**:5498–503.

10 Tagawa Y, Sekikawa K, Iwakura Y. Suppression of concanavalin A-induced hepatitis in IFN-gamma(−/−) mice, but not in TNF-alpha(−/−) mice: role for IFN-gamma in activating apoptosis of hepatocytes. *J Immunol* 1997; **159**:1418–28.

11 Toyabe S, Seki S, Iiai T *et al.* Requirement of IL-4 and liver NK1+ T cells for concanavalin A-induced hepatic injury in mice. *J Immunol* 1997; **159**:1537–42.

12 Massaguer A, Perez-Del-Pulgar S, Engel P, Serratosa J, Bosch J, Pizcueta P. Concanavalin-A-induced liver injury is severely impaired in mice deficient in P-selectin. *J Leukoc Biol* 2002; **72**:262–70.
13 Diao H, Kon S, Iwabuchi K *et al.* Osteopontin as a mediator of NKT cell function in T cell-mediated liver diseases. *Immunity* 2004; **21**:539–50.
14 Anand S, Wang P, Yoshimura K *et al.* Essential role of TNF family molecule LIGHT as a cytokine in the pathogenesis of hepatitis. *J Clin Invest* 2006; **116**:1045–51.
15 Adachi M, Watanabe-Fukunaga R, Nagata S. Aberrant transcription caused by the insertion of an early transposable element in an intron of the Fas antigen gene of lpr mice. *Proc Natl Acad Sci USA* 1993; **90**:1756–60.
16 Watanabe-Fukunaga R, Brannan CI, Copeland NG, Jenkins NA, Nagata S. Lymphoproliferation disorder in mice explained by defects in Fas antigen that mediates apoptosis. *Nature* 1992; **356**:314–7.
17 Komori H, Furukawa H, Mori S *et al.* A signal adaptor SLAM-associated protein regulates spontaneous autoimmunity and Fas-dependent lymphoproliferation in MRL-Faslpr lupus mice. *J Immunol* 2006; **176**:395–400.
18 Yang JQ, Singh AK, Wilson MT *et al.* Immunoregulatory role of CD1d in the hydrocarbon oil-induced model of lupus nephritis. *J Immunol* 2003; **171**:2142–53.
19 Yang JQ, Saxena V, Xu H, Van KaerL, Wang CR, Singh RR. Repeated alpha-galactosylceramide administration results in expansion of NK T cells and alleviates inflammatory dermatitis in MRL-lpr/lpr mice. *J Immunol* 2003; **171**: 4439–46.
20 Veillette A. NK cell regulation by SLAM family receptors and SAP-related adapters. *Immunol Rev* 2006; **214**:22–34.
21 Veillette A. Immune regulation by SLAM family receptors and SAP-related adaptors. *Nat Rev Immunol* 2006; **6**:56–66.
22 Kawachi I, Maldonado J, Strader C, Gilfillan S. MR1-restricted V alpha 19i mucosal-associated invariant T cells are innate T cells in the gut lamina propria that provide a rapid and diverse cytokine response. *J Immunol* 2006; **176**: 1618–27.
23 Croxford JL, Miyake S, Huang YY, Shimamura M, Yamamura T. Invariant V(alpha)19i T cells regulate autoimmune inflammation. *Nat Immunol* 2006; **7**:987–94.

Genetic classification of ovarian carcinoma based on microsatellite analysis: Relationship to clinicopathological features and patient survival

ZHANG HUAN[1,4], KENTARO NAKAYAMA[1], NAOMI NAKAYAMA[1], MASAKO ISHIBASHI[1], SHAMIMA YEASMIN[1], ATSUKO KATAGIRI[1], INDRI NURYANI PURWANA[1], KOUJI IIDA[1], RIRUKE MARUYAMA[3], MANABU FUKUMOTO[2] and KOHJI MIYAZAKI[1]

[1]Department of Obstetrics and Gynecology, Shimane University School of Medicine, Izumo; [2]Department of Pathology Institute of Development, Aging and Cancer, Tohoku University, Sendai; [3]Department of Pathology Shimane University School of Medicine, Izumo, Japan; [4]Department of Gynecology and Obstetrics, The Affiliated Hospital of Ningxia Medical College, P.R. China

Received June 29, 2007; Accepted September 28, 2007

Abstract. Ovarian carcinomas can progress through two pathways of genomic instability: chromosomal instability (CIN) and microsatellite instability (MSI). However, it is unknown whether these two mechanisms could be distinguished from each other in the molecular characteristics in ovarian carcinomas. We hypothesized that these two pathways are not always independent in ovarian carcinomas. We classified 51 ovarian carcinomas based on their MSI and CIN status using microsatellite analysis and assessed whether these carcinogenic pathways affect the clinicopathological features and patient survival. Of the 51 cases, 77.4% of the tumors were microsatellite stable (MSS), 5.9% were MSI-Low (MSI-L) whilst, 16.7% were MSI-High (MSI-H). Overall, 56.8% of the tumors had at least one loss of heterozygosity (LOH) event, i.e., 56.8% CIN. Notably, we identified a significant degree of overlap between the MSI and CIN pathways. Of the 34 tumors with LOH events (CIN), 5 (14.7%) were MSI-H. In addition, of the 7 tumors that were MSI-H, 5 (71.4%) had one or more LOH events (CIN). We also identified a group of 29.4% of all tumors that did not demonstrate any evidence of either of the two pathways of genomic instability as they were MSS/MSI-L with no evidence of LOH events (CIN negative). Furthermore, patients with CIN with MSS/MSI-L have a significantly shorter overall survival compared to those in other genetic categories (P=0.019). Cox regression analysis revealed that tumors with CIN with MSS/MSI-L exhibit a poor prognostic outcome after adjustment for FIGO stage and grade. These findings suggest that some ovarian carcinomas have a significant degree of overlap between the two pathways of genomic instability and that the genetic classification using microsatellite markers may represent a potential new biomarker of risk prediction in ovarian carcinoma.

Correspondence to: Dr Kentaro Nakayama, Department of Obstetrics and Gynecology, Shimane University School of Medicine, Enyacho 89-1, Izumo 693-8501, Japan
E-mail: kn88@med.shimane-u.ac.jp

Abbreviations: LOH, loss of heterozygosity; CIN, chromosomal instability; MSI, microsatellite instability; MSS, microsatellite stable; MMR, mismatch repair

Key words: ovarian carcinoma, loss of heterozygosity, microsatellite instability, genomic instability, prognosis

Introduction

Ovarian carcinoma is the most lethal gynecological malignancy at present (1). Women with organ-confined tumors have an excellent prognosis, whereas the overall survival of the majority of ovarian carcinoma patients with advanced disease is <30% (2,3). Despite the development of new therapeutic approaches, these survival statistics have remained largely unchanged for many years. Clearly, there is a need for a better understanding of the molecular pathogenesis of ovarian carcinoma so that new drug targets or biomarkers that facilitate risk prediction can be identified.

Ovarian carcinogenesis is characterized by the successive accumulation of mutations in genes controlling epithelial cell growth and differentiation. The term 'genomic instability' describes conditions in which widespread loss of DNA integrity is perpetuated. The development of genomic instability is an important event in the multistep progression of ovarian carcinogenesis. Two apparently independent pathways of genomic instability have been identified (4,5). The first, and more common pathway is characterized by the sequential inactivation of tumor-suppressor genes, such as *p53* (chromosome 17p), *BRCA1* (chromosome 17q) and *FHIT* (chromosome 3p). Tumors generated through this

'suppressor' pathway display chromosal instability (CIN) with frequent cytogenetic abnormalities and allelic losses (6,7). The precise mechanism driving the process of chromosomal instability is not completely understood. A second pathway is characteristic of tumors from patients with HNPCC, an autosomal-dominat condition that accounts for 2-3% of all colorectal carcinomas. The hallmark of this alternative 'mutator' pathway is widespread microsatellite instability (MSI), which is characterized by the accumulation of somatic alterations in the length of simple, repeated nucleotide sequences called 'microsatellites'.

Microsatellite instability (MSI) is also seen in a significant proportion of extracolonic tumors including breast, endometrial (8), gastric (9), and ovarian carcinoma (10-12). MSI-H has also been identified in 3-10% of sporadic solid carcinomas (13). In these cases, mutations of *hMLH1* and *hMSH2* are rarely found. Some studies indicate that *hMLH1* inactivation by promoter hypermethylation also produces the MSI-H phenotype in sporadic solid carcinomas and is responsible for most, if not all, of the sporadic solid carcinomas exhibiting MSI-H (14-16). MSI-H colorectal carcinomas do not exhibit gross cytogenetic abnormalities; and they are not generally aneuploid (17,18). Furthermore, patients with MSI-H tumors have a more favorable survival compared to patients with MSI-L/MSS solid carcinomas (13,19,20).

Although these two mechanisms of genomic instability can be distinguished from one another by their molecular characteristics, current evidence suggests that there might be some degree of overlap. Recently, Goel *et al* reported that there is a significant degree of overlap between the MSI and CIN pathways in colorectal carcinomas (21). To date, no systematic study has determined the extent of overlap between the MSI and CIN pathways in ovarian carcinomas. The present study was therefore pursued in order to classify ovarian carcinomas based on their MSI and CIN status. We hypothesized that some tumors would exhibit a significant degree of overlap between these two mechanisms, whilst a proportion of tumors might not show any evidence for involvement of either mutational pathways. In addition, we assessed whether evidence of these carcinogenic pathways was related to clinicopathological features and patient survival.

Materials and methods

Patients and tumor samples. Fifty-one ovarian carcinomas and their adjacent non-neoplastic tissues were obtained from archival pathological specimens from the Shimane University Hospital in Japan. Written informed consent for the analysis in this study was obtained for each individual case. Acquisition of tissue specimens was approved by the Institutional Review Board at Shimane University. Diagnostic verification, tumor subtyping and grading were performed independently by two certified pathologists (R.M. and M.F.). Ovarian carcinomas were diagnosed on the basis of conventional histopathological criteria (22), using the grading criteria recommended by the International Federation of Gynecology and Obstetrics.

The series of tumor tissues included in the study consisted of 20 serous, 17 mucinous, 11 endometrioid and 3 clear cell ovarian carcinomas. The 51 tumors included 24 well-differentiated (grade 1), 14 moderately differentiated (grade 2) and 13 poorly differentiated (grade 3) ovarian carcinomas. There were 22 stage I patients, 5 stage II patients, 19 stage III patients and 5 stage IV patients in this study.

Patients had no other malignancies and had performance status of grade 0 or 1. All patients were primarily treated with cytoreductive surgery and postoperative chemotherapy, which consisted of 6-12 courses of a paclitaxel-carboplatin regimen (TC; paclitaxel 175mg/m^2, CBDCA AUC5). Chemotherapy response was assessed by second-look surgery or by clinical and/or radiographic evaluation according to the WHO criteria. Patients with incomplete responses to induction chemotherapy or with recurrent tumors, were treated with a variety of second-line chemotherapy regimens. Follow-up for all patients included in the survival analysis was updated June 25, 2003 (median follow-up time was 80 months; range, 50-120 months). At that time, 27 patients had died of ovarian carcinoma.

DNA extraction using microdissection and PCR amplification. Paraffin-embedded tissues were sectioned at a thickness of 5 μm and stained with hematoxylin and eosin. The cancerous and non-neoplastic portions were collected separately with a 29-gauge needle using an MK1 micromanipulator (Singer Instruments, Roadwater, UK) under a dissecting microscope. The dissected tissue was collected in an Eppendorf tube and incubated overnight at 58°C in a digestion mixture (0.01 M NaCl; 0.5 M Tris-HCl, pH 8.0; 20 mM EDTA; 0.05% Tween-20®; 0.1 mg/ml proteinase K). The samples were then heated to 95°C for 10 min to inactivate the proteinase K activity. After digestion, DNA was extracted with phenol/chloroform treatment and ethanol precipitation. PCR reactions were performed in a total volume of 10 μl containing 25-50 ng of DNA, dNTPs at a final concentration of 20 μM, 0.4 μM of each primer, and 0.25 units of *Ex-Taq* DNA polymerase (Takara Shuzo, Shiga, Japan) or Platinum *Taq* DNA polymerase (Gibco Brl, Rockville, MD). After the mixture was heated for 10 min at 94°C, PCR was performed for 45 cycles at 94°C, at the appropriate annealing temperature and at 72°C for 1 min each, followed by 72°C for 10 min. After denaturation of the PCR products at 94°C for 2 min, samples were subjected to electrophoresis using Performance optimized polymer 4 in a 310 Genetic analyzer (Applied Biosystems, Foster, CA). LOH analysis was performed by Gene Scan version 2.1.

Microsatellite markers and MSI analysis. Allelic imbalances were measured by performing MSI on all matched normal and tumor tissues by PCR amplification. A panel of eight microsatellite markers with dye-labeled primers, comprising of 7 dinucleotide repeats (D2S123, D5S346, D8S87, D13S153, D13S175, D18S55, D20S100) and, 1 mononucleotide repeat (BAT25) were used to determine tumor MSI status. These markers included the recommended markers for the detection of MSI proposed at the National Cancer Institute collaborative meeting on MSI in colorectal carcinoma (23). Loci were scored according to the published guidelines. Changes in the electrophoretic mobility of DNA amplified by PCR were used to assess the MSI. We defined tumors as exhibiting MSI if they had at least 1 locus with MSI among cases in which PCR was successful on more than

Table I. Association of microsatellite genotypes with clinicopathological features.

	CIN n=34	CIN negative n=17	MSI-H n=7	MSI-L/MS n=47	P-value
Histological type					
Serous (n=20)	13	10	1	22	0.07[a]
Mucinous (n=17)	12	4	2	14	
Endometrioid (n=11)	6	3	4	5	
Clear (n=3)	3	0	0	3	
Grade					
Well (n=24)	12	11	6	17	0.02[b]
Moderate (n=14)	11	2	0	13	
Poor (n=13)	11	4	1	14	
FIGO stage/TNM stage					
I/Tl (n=22)	12	9	5	16	0.04[c]
II/T2 (n=5)	2	3	1	4	0.04[d]
III/T3 (n=19)	17	4	1	20	
IV/T4 (n=5)	3	1	0	4	

[a]MSI-H tumors tended to be more frequent in endometrioid type tumors than in serous type tumors. [b]MSI-H tumors were significantly more frequent in well differentiated carcinomas than in moderately/poorly differentiated carcinomas. [c]MSI-H tumors were significantly more frequent in stage I, II tumors than in stage III, IV tumors. [d]IN tumors were significantly more frequent in stage III, IV tumors than in stage I, II tumors.

five loci. Among tumors exhibiting MSI, cases with >30% of loci showing MSI were defined as MSI-H and the remaining cases were designated MSI-L. Tumors not demonstrating allelic shifts were termed as MSS (Fig. 1).

Microsatellite markers and LOH analysis. Eight sets of polymorphic microsatellite sequences that are tightly linked to known tumor suppressor genes and markers reported to be associated with ovarian carcinoma were used to identify significant allelic losses in the carcinoma specimens. DNA was amplified by PCR using dye-labeled primers at microsatellite loci linked to the *FHIT* locus on 3p21.2-14.2 (D3S1306), *p53* locus on 17p13 (TP53), *BRCA1* locus on 17q21 (D17S579), 6q25 (D6S473), 7q31 (D7S523), 9q31-33 (D9S59), 11p15.5-15.3 (D11S988) and Xq11-12 (AR). LOH was quantified by calculating the LOH index. This was defined as the allele ratio in normal tissue divided by the allele ratio in tumor tissue. The allele ratio was calculated as the peak height of the smaller allele divided by the peak height of the larger allele. If the LOH index was <0.5 or >2.0, we defined the case as LOH. The LOH frequency of each locus was represented by the ratio of the number of cases with LOH to the total number of informative cases.

Statistical analysis. Overall survival time was measured in months from the time of surgery to the reported death. Survival curves were determined using the Kaplan-Meier method and differences in survival between subgroups were compared with the log-rank test. P-values <0.05 were considered significant. All reported P-values are two-tailed.

Results

Microsatellite typing. Informative results were obtained for all tumor specimens. Of the 51 cases, 41 (77.4%) were MSS, 3 (5.9%) were MSI-L, and 7 (16.7%) were MSI-H (Table I). MSI-L tumors were categorized along with MSS tumors for all statistical purposes in this study. MSI-H tumors correlated with both histological subtype and tumor grade. MSI-H tumors tended to be more frequent in endometrioid type tumors than in serous type tumors (P=0.07) (Table I). In addition, MSI-H tumors were significantly more frequent in well-differentiated carcinomas than in moderately/poorly differentiated carcinomas (P=0.02). MSI-H tumors were significantly more frequent in stage I, II tumors than in stage III, IV tumors (P=0.04).

LOH study. We identified 34 tumors (66.7%) with LOH at one or more of the eight loci studied. Overall, the frequency of LOH in tumors with any LOH event was most common in 17p13 (TP53) (46.3%), followed by 11p15.5-15.3 (D11S988) (38.7%), 3p21.2-14.2 (D3S1306) (34.8%), 9q31-33 (D9S59) (30.0%), 7q31 (D7S523) (29.4%), 6q25 (D6S473) (21.0%), Xq11-12 (AR) (15.0%) and 17q21 (D17S579) (13.2%). Based on the number of affected LOH, the LOH genotype was divided into 2 groups. Tumors with LOH in at least one of the eight markers were classified as exhibiting chromosomal instability (CIN) whilst tumors with no evidence of LOH were classified as CIN negative. Of the 53 cases, 34 (66.7%) were CIN positive and 17 (33.3%) were CIN negative (Table I). CIN tumors were significantly more frequent in stage III, IV tumors than in stage I, II tumors (P=0.04).

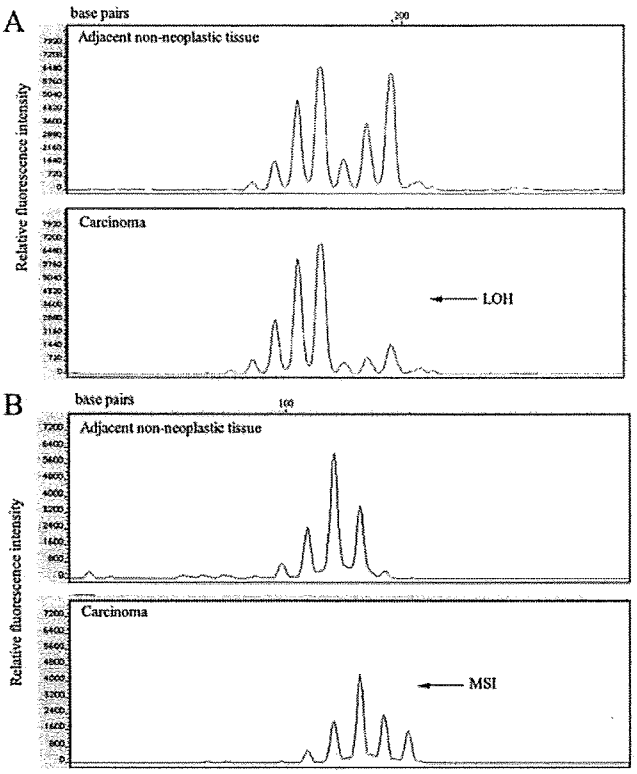

Figure 1. Representative example of the loss of heterozygosity (LOH) and microsatellite instability (MSI).

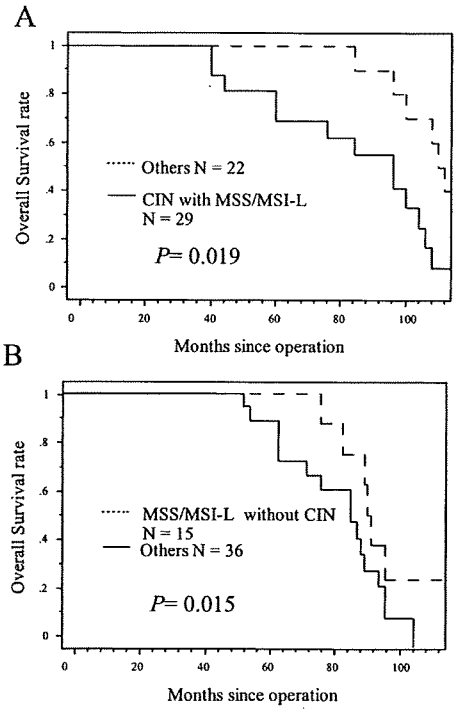

Figure 3. Kaplan-Meier curves of 51 ovarian carcinomas according to the status of genomic instability. (A) Patients with CIN with MSS/MSI-L have a significantly shorter overall survival compared with other genetic categories (P=0.019). (B) Patients with MSS/MSI-L without CIN tended to have a favorable overall survival compared with other genetic categories (P=0.151).

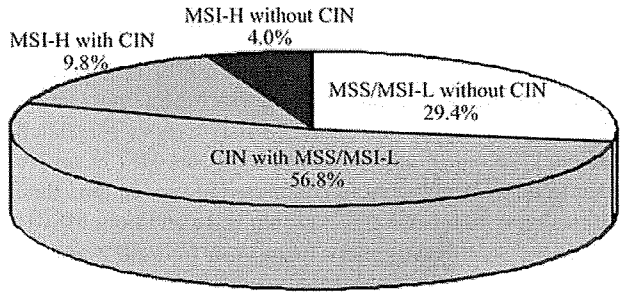

Figure 2. Exclusiveness and overlap among subsets of genomic instability. Summary of genomic instability patterns for 51 ovarian carcinomas.

Overlap of different pathways of genomic instability. We then investigated the degree of overlap between tumors with CIN and those with MSI. Of the 34 tumors with evidence of CIN, 85.3% were MSS/MSI-L and 14.7% were MSI-H (Table I). Of the 44 MSS/MSI-L tumors, 65.9% also contained a LOH event at one or more of the loci tested (CIN), as did 71.4% of the MSI-H tumors. The proportions of CIN positive tumors did not differ according to MSI status. We also examined the distribution of tumors that exhibited the following combinations: CIN and MSS/MSI-L, CIN and MSI-H, MSI-H without CIN, and MSS/MSI-L without CIN (Fig. 2). We found that 9.8% of all tumors exhibited both MSI-H and CIN whilst, 4.0% were negative for both MSI-H and CIN. In addition, 56.8% of the MSS/MSI-L tumors were CIN negative. It is noteworthy that we identified a group comprising of 29.4% of all tumors examined that were MSS/MSI-L and CIN negative and therefore did not demonstrate signs of either of the two pathways of genomic instability (Fig. 2).

Correlation between status of genomic instability and clinicopathological features. Comparisons of the clinical and pathological variables of these four tumor categories are provided in Table II. There was no significant difference in the relationship between the status of genomic instability and histological subtype. With respect to the histological grade, a significantly greater fraction of tumors with CIN with MSS/MSI-L were observed in well-differentiated carcinomas compared with tumors exhibiting MSS/MSI-L without CIN (P=0.034, 0.036; well vs moderate, well vs moderate + poor). Patients were grouped as early stage (stage I and II) and advanced stage (stage III and IV) carcinomas. We found that 19 out of 29 CIN positive tumors with MSS/MSI-L types (65.5%) were advanced stage. On the other hand, 10 out of 15 CIN negative tumors with MSS/MSI-L types (66.7%), 4 out of 5 CIN positive tumors with MSI-H types (80.0%) and 2 out of 2 CIN negative tumors with MSI-H types (100%) were more common in the early stage. CIN positive tumors with MSS/MSI-L types exhibited a significantly more advanced stage compared with CIN negative tumors with MSS/MSI-L types (P=0.042).

Analysis of survival rate. To verify whether a specific genomic instability exhibits a preferential association with more or less

Table II. Correlation between status of genomic instability and clinicopathological features.

	CIN with MSS/MSI-L (n=29)	MSI-H without CIN (n=2)	MSI-H with CIN (n=5)	MSS/MSI-L without CIN (n=15)	Total (n=51)	P-value
Histological type						
Serous (n=20)	13	1	0	9	20	
Mucinous (n=17)	10	0	2	4	17	
Endometrioid (n=11)	3	1	3	2	11	
Clear (n=3)	3	0	0	0	3	
Grade						
Well (n=24)	8	2	4	9	24	0.034[a]
Moderate (n=14)	11	0	0	2	14	0.036[b]
Poor (n=13)	10	0	1	4	13	
FIGO stage/TNM stage						
I/T1 (n=22)	9	2	3	7	22	0.042[c]
II/T2 (n=5)	1	0	1	3	5	
III/T3 (n=19)	16	0	1	4	19	
IV/T4 (n=5)	3	0	0	1	5	

[a,b]A significantly greater fraction of tumors with CIN with MSS/MSI-L were observed in well-differentiated carcinomas compared with tumors exhibiting MSS/MSI-L without CIN (well vs moderate, well vs moderate + poor). [c]CIN with MSS/MSI-L tumors exhibited a significantly more advanced stage compared with MSS/MSI-L without CIN tumors.

Table III. Multivariate analysis of overall survival in ovarian carcinoma patients.

	Univariate	Multivariate		
Variables	P-value	Hazard ratio	95% CI	P-value
FIGO stage I, II (n=27) vs III, IV (n=24)	0.0003	7	1.2-38.7	0.027
Histological grade Poorly differentiated (n=13) vs Others (n=38)	0.0126	1.6	0.3-7.5	0.545
Status of genomic instability CIN with MSS/MSI-L (n=29) vs Others (n=22)	0.02	2.5	1.0-6.0	0.042

favorable clinical course, the overall survival of patients with all genetic categories were analyzed using the Kaplan-Meier method. We analyzed the overall survival in CIN-positive tumors with CIN-negative tumors and MSI-H tumors with MSS/MSI-L tumors. The patients with CIN-positive tumors tended to have a shorter overall survival compared to those with CIN-negative tumors (P=0.099). In contrast, MSI-H had no influence on patient survival (P=0.421). Then, we compared overall survival of the four categories described above (i.e., CIN with MSS/MSI-L, MSI-H without CIN, MSI-H with CIN and MSS/MSI-L without CIN). Patients with CIN with MSS/MSI-L had a significantly shorter overall survival compared with other genetic categories (P=0.019) (Fig. 3A). However, patients with MSS/MSI-L without CIN tended to have a more favorable overall survival compared with other genetic categories (P=0.151) (Fig. 3B). No statistically significant difference was evident in the survival curves of patients with the other two genetic classifications (P=0.644 and 0.838, respectively). To determine whether CIN-positive tumors with MSS/MSI-L were a prognostic marker independent of FIGO stage or histological grade established prognostic markers, we conducted an overall survival analysis using the Cox proportional hazards model (Table III). FIGO stage (hazard ratio: 7.0, 95% CI: 1.2-38.7, P=0.027) and CIN with MSS/MSI-L (hazard ratio: 2.5, 95% CI: 1.0-6.0, P=0.042) were independent prognostic factors in patients with ovarian carcinoma (Table III).

Discussion

Our current understanding of solid tumor carcinogenesis, including ovarian carcinoma suggests that at least two mechanisms are capable of producing the mutations required for a cell to demonstrate a malignant phenotype. These mechanisms include CIN, characterized in tumor DNA by the presence of multiple LOH events, and loss of MMR function that is defined by high levels of MSI. In the current study, we examined 51 cases of ovarian carcinoma to determine whether

these two mechanisms of tumorigenesis operated independently or whether there exists a significant degree of overlap.

We defined tumors as MSI if they had at least 1 locus with MSI among cases in which PCR was successful at more than 5 loci. Among MSI tumors, cases with >30% of loci showing MSI were defined as MSI-H and the remaining cases were designated MSI-L. Some studies suggest that the molecular profiles of MSS and MSI-L tumors are indistinguishable (24,25) and we therefore, categorized MSI-L tumors with MSS tumors for all statistical purposes. To investigate allelic losses by LOH, we used eight polymorphic markers mapped closely to key tumor suppressor genes that are believed to be lost during ovarian carcinogenesis (26-32). Detection of LOH in at least one of these sites was taken as evidence of loss of tumor suppressor activity by CIN. We accept that it is possible and even likely that tumors may well be reclassified by the addition of markers outside the usual deletion sites. However, without a single LOH event at the eight sites examined, it is highly unlikely that a tumor would exhibit widespread LOH that is characteristic of tumors arising in the setting of CIN. With these data, we classified the tumors as belonging to one of four genotypes: CIN with MSS/MSI-L; CIN with MSI-H; MSI-H without CIN and MSS/MSI-L without CIN.

MSI-H without CIN was found in 4% of the tumors analyzed. MSI-H is caused by a defect in DNA MMR capability which is most commonly caused by hypermethylation of the hMLH1 promoter (33). Carcinomas associated with MMR defect are typically diploid, although comparative genomic hybridization shows that these tumors may also demonstrate amplifications and deletions of single alleles or chromosomes (34). In agreement with this, 9.8% of the tumors in our study exhibited both MSI-H and CIN.

CIN, as evidenced by allelic loss at one or more of the eight markers tested, was observed in 66.7% of the tumors examined. Tumors that exhibited LOH without MSI-H comprised 56.8% of the tumors. The presumed course of tumor progression in this subset involves accumulated allelic losses at the tumor suppressor loci (4). The processes responsible for CIN are unknown. Many mechanistic explanations have been offered for CIN, but none have been shown to be sufficient to account for this process in solid tumor carcinogenesis (7,35,36). It is likely that multiple causes of CIN will be discovered through the study of these and other events in early carcinogenesis.

The most intriguing subgroup identified in this study was the 29.4% of ovarian carcinomas that lacked any evidence of either CIN or MSI. The molecular events leading to the development of carcinomas in this subgroup with no signs of genomic instability are unknown. One reasonable possibility is the transcriptional silencing of growth and differentiation genes by epigenetic modification. Aberrant promoter methylation, leading to loss of the tumor suppressor function, has been observed in a variety of cancers (37). Epigenetic modification of tumor suppressor genes is characteristically age dependent (38) and there are several reports in the literature regarding tumor-specific methylation patterns (39). We are in the process of characterizing the MSS/MSI-L without CIN subset using methylation-specific PCR.

We then assessed whether these carcinogenic pathways as discussed above, affect the clinical prognosis. It is well accepted that clinical stage is the most reliable guide to a prognosis. A biomarker might provide additional prognostic information if it were directly linked to a mechanism driving invasion and metastasis. Many investigators reported that MSI solid carcinomas are associated with an improved prognosis (13,19,20), but the reasons are unclear (40). In the current study, MSI ovarian carcinomas had no influence on patient survival (P=0.421). The emergence of carcinoma cells that are resistant to cisplatin and carboplatin is a major clinical problem and often leads to tumor recurrence (41). Ovarian carcinoma cell lines that develop resistance to cisplatin have been found to acquire an MSI-H phenotype (42). Therefore, MSI-H ovarian carcinomas might not be associated with an improved prognosis in this study because all ovarian carcinoma patients in this study received cisplatin based chemotherapy.

One of the most statistically significant findings in our study was that patients with CIN with MSS/MSI-L ovarian carcinomas had a poor prognosis. CIN can be interpreted as indicating a high level of deleted chromosomal regions, aberrant mitotic recombinations, or nondisjunctional chromosomal loss (43). In addition, it is also possible that some of the allelic imbalances we observed were due to the amplification of certain chromosomal regions. While genetic instability has generally been considered to be a characteristic feature of malignancy, it is still a matter of debate whether this instability is causally related to carcinogenesis or merely the result of other cellular events. Recent studies of colon carcinoma cells exhibiting CIN indicated that the CIN phenotype appeared to be a causative factor for tumor development, and may result from defects in proteins participating in mitotic checkpoint control (6). The striking association between tumors with CIN with MSS/MSI-L and a poor prognosis, as observed in our study, may be explained by the possibility that CIN reflects an aggressive tumor phenotype. Our findings appear to fit the concept that specific types of genetic instability exist, and that this instability has a role in driving tumor development and progression (44).

In summary, we reported that some ovarian carcinomas have a significant degree of overlap between the two pathways of genomic instability: CIN and MSI. The results of our study suggest that microsatellite typing is a useful tool for the construction of a comprehensive genetic classification that aims to predict the diverse clinical prognosis. A genetic classification using microsatellite markers may represent a potential new biomarker of risk prediction in ovarian carcinoma.

References

1. Wingo PA, Tong T and Bolden S: Cancer statistics, 1995. CA Cancer J Clin 45: 8-30, 1995.
2. Landis SH, Murray T, Bolden S and Wingo PA: Cancer statistics, 1999. CA Cancer J Clin 49: 8-31, 1999.
3. Holschneider CH and Berek JS: Ovarian cancer: epidemiology, biology, and prognostic factors. Semin Surg Oncol 19: 3-10, 2000.
4. Kinzler KW and Vogelstein B: Lessons from hereditary colorectal cancer. Cell 87: 159-170, 1996.
5. Toft NJ and Arends MJ: DNA mismatch repair and colorectal cancer. J Pathol 185: 123-129, 1998.
6. Lengauer C, Kinzler KW and Vogelstein B: Genetic instabilities in human cancers. Nature 396: 643-649, 1998.

7. Cahill DP, Lengauer C, Yu J, Riggins GJ, Willson JK, Markowitz SD, *et al*: Mutations of mitotic checkpoint genes in human cancers. Nature 392: 300-303, 1998.
8. Gurin CC, Federici MG, Kang L and Boyd J: Causes and consequences of microsatellite instability in endometrial carcinoma. Cancer Res 59: 462-426, 1999.
9. Leung WK, Kim JJ, Kim JG, Graham DY and Sepulveda AR: Microsatellite instability in gastric intestinal metaplasia in patients with and without gastric cancer. Am J Pathol 156: 537-543, 2000.
10. Sood AK and Buller RE: Genomic instability in ovarian cancer: a reassessment using an arbitrarily primed polymerase chain reaction. Oncogene 13: 2499-2504, 1996.
11. Hickey KP, Boyle KP, Jepps HM, Andrew AC, Buxton EJ and Burns PA: Molecular detection of tumour DNA in serum and peritoneal fluid from ovarian cancer patients. Br J Cancer 80: 1803-1808, 1999.
12. Sood AK, Holmes R, Hendrix MJ and Buller RE: Application of the National Cancer Institute international criteria for determination of microsatellite instability in ovarian cancer. Cancer Res 61: 4371-4374, 2001.
13. Lawes DA, SenGupta S and Boulos PB: The clinical importance and prognostic implications of microsatellite instability in sporadic cancer. Eur J Surg Oncol 29: 201-212, 2003.
14. Cunningham JM, Christensen ER, Tester DJ, Kim CY, Roche PC, Burgart LJ, *et al*: Hypermethylation of the hMLH1 promoter in colon cancer with microsatellite instability. Cancer Res 58: 3455-3460, 1998.
15. Kuismanen SA, Holmberg MT, Salovaara R, Schweizer P, Aaltonen LA, de La Chapelle A, *et al*: Epigenetic phenotypes distinguish microsatellite-stable and -unstable colorectal cancers. Proc Natl Acad Sci USA 96: 12661-12666, 1999.
16. Murata H, Khattar NH, Kang Y, Gu L and Li GM: Genetic and epigenetic modification of mismatch repair genes hMSH2 and hMLH1 in sporadic breast cancer with microsatellite instability. Oncogene 21: 5696-5703, 2002.
17. Olschwang S, Hamelin R, Laurent-Puig P, Thuille B, De Rycke Y, Li YJ, *et al*: Alternative genetic pathways in colorectal carcinogenesis. Proc Natl Acad Sci USA 94: 12122-12127, 1997.
18. Eshleman JR, Casey G, Kochera ME, Sedwick WD, Swinler SE, Veigl ML, *et al*: Chromosome number and structure both are markedly stable in RER colorectal cancers and are not destabilized by mutation of p53. Oncogene 17: 719-725, 1998.
19. Bubb VJ, Curtis LJ, Cunningham C, Dunlop MG, Carothers AD, Morris RG, *et al*: Microsatellite instability and the role of hMSH2 in sporadic colorectalcancer. Oncogene 12: 2641-2649, 1996.
20. Watson P, Lin KM, Rodriguez-Bigas MA, Smyrk T, Lemon S, Shashidharan M, *et al*: Colorectal carcinoma survival among hereditary nonpolyposis colorectal carcinoma family members. Cancer 83: 259-266, 1998.
21. Goel A, Arnold CN, Niedzwiecki D, Chang DK, Ricciardiello L, Carethers JM, *et al*: Characterization of sporadic colon cancer by patterns of genomic instability. Cancer Res 63: 1608-1614, 2003.
22. Serov SF, Scully RE and Sobin LH: Histopathological typing of ovarian tumors: International classification of tumors. Vol. 9, WHO, Geneva, 1973.
23. Boland CR, Thibodeau SN, Hamilton SR, Sidransky D, Eshleman JR, Burt RW, *et al*: A National Cancer Institute Workshop on Microsatellite Instability for cancer detection and familial predisposition: development of international criteria for the determination of microsatellite instability in colorectal cancer. Cancer Res 58: 5248-5257, 1998.
24. Kambara T, Matsubara N, Nakagawa H, Notohara K, Nagasaka T, Yoshino T, *et al*: High frequency of low-level microsatellite instability in early colorectal cancer. Cancer Res 61: 7743-7746, 2001.
25. Halford S, Sasieni P, Rowan A, Wasan H, Bodmer W, Talbot I, *et al*: Low-level microsatellite instability occurs in most colorectal cancers and is a nonrandomly distributed quantitative trait. Cancer Res 62: 53-57, 2002.
26. Fullwood P, Marchini S, Rader JS, Martinez A, Macartney D, Broggini M, *et al*: Detailed genetic and physical mapping of tumor suppressor loci on chromosome 3p in ovarian cancer. Cancer Res 59: 4662-4667, 1999.
27. Colitti CV, Rodabaugh KJ, Welch WR, Berkowitz RS and Mok SC: A novel 4 cM minimal deletion unit on chromosome 6q25.1-q25.2 associated with high grade invasive epithelial ovarian carcinomas. Oncogene 16: 555-559, 1998.
28. Koike M, Takeuchi S, Yokota J, Park S, Hatta Y, Miller CW, *et al*: Frequent loss of heterozygosity in the region of the D7S523 locus in advanced ovarian cancer. Genes Chromosomes Cancer 19: 1-5, 1997.
29. Devlin J, Elder PA, Gabra H, Steel CM and Knowles MA: High frequency of chromosome 9 deletion in ovarian cancer: evidence for three tumour-suppressor loci. Br J Cancer 73: 420-423, 1996.
30. Lu KH, Weitzel JN, Kodali S, Welch WR, Berkowitz RS and Mok SC: A novel 4-cM minimally deleted region on chromosome 11p15.1 associated with high grade nonmucinous epithelial ovarian carcinomas. Cancer Res 57: 387-390, 1997.
31. Wertheim I, Tangir J, Muto MG, Welch WR, Berkowitz RS, Chen WY, *et al*: Loss of heterozygosity of chromosome 17 in human borderline and invasive epithelial ovarian tumors. Oncogene 12: 2147-2153, 1996.
32. Edelson MI, Lau CC, Colitti CV, Welch WR, Bell DA, Berkowitz RS, *et al*: A one centimorgan deletion unit on chromosome Xq12 is commonly lost in borderline and invasive epithelial ovarian tumors. Oncogene 16: 197-202, 1998.
33. Herman JG, Umar A, Polyak K, Graff JR, Ahuja N, Issa JP, *et al*: Incidence and functional consequences of hMLH1 promoter hypermethylation in colorectal carcinoma. Proc Natl Acad Sci USA 95: 6870-6875, 1998.
34. Georgiades IB, Curtis LJ, Morris RM, Bird CC and Wyllie AH: Heterogeneity studies identify a subset of sporadic colorectal cancers without evidence for chromosomal or microsatellite instability. Oncogene 18: 7933-7940, 1999.
35. Jallepalli PV, Waizenegger IC, Bunz F, Langer S, Speicher MR, Peters JM, *et al*: Securin is required for chromosomal stability in human cells. Cell 105: 445-457, 2001.
36. Nathke IS: The adenomatous polyposis coli protein. Mol Pathol 52: 169-173, 1999.
37. Toyota M, Ho C, Ahuja N, Jair KW, Li Q, Ohe-Toyota M, *et al*: Identification of differentially methylated sequences in colorectal cancer by methylated CpG island amplification. Cancer Res 59: 2307-2312, 1999.
38. Ahuja N, Li Q, Mohan AL, Baylin SB and Issa JP: Aging and DNA methylation in colorectal mucosa and cancer. Cancer Res 58: 5489-5494, 1998.
39. Esteller M, Corn PG, Baylin SB and Herman JG: A gene hypermethylation profile of human cancer. Cancer Res 61: 3225-3229, 2001.
40. Lynch HT, Smyrk T and Lynch JF: Overview of natural history, pathology, molecular genetics and management of HNPCC (Lynch Syndrome). Int J Cancer 69: 38-43, 1996.
41. Kavanagh J, Tresukosol D, Edwards C, Freedman R, Gonzalez de Leon C, Fishman A, *et al*: Carboplatin reinduction after taxane in patients with platinum-refractory epithelial ovarian cancer. J Clin Oncol 13: 1584-1588, 1995.
42. Anthoney DA, McIlwrath AJ, Gallagher WM, Edlin AR and Brown R: Microsatellite instability, apoptosis, and loss of p53 function in drug-resistant tumor cells. Cancer Res 56: 1374-1381, 1996.
43. Gupta PK, Sahota A, Boyadjiev SA, Bye S, Shao C, O'Neill JP, *et al*: High frequency in vivo loss of heterozygosity is primarily a consequence of mitotic recombination. Cancer Res 57: 1188-1193, 1997.
44. Cahill DP, Kinzler KW, Vogelstein B and Lengauer C: Genetic instability and darwinian selection in tumours. Trends Cell Biol 9: M57-M60, 1999.

ExHFT-7
28 June – 03 July 2009, Krakow, Poland

ACOUSTIC CHARACTERISTICS OF ULTRASOUND IN WATER CONTAINING LIPID MICROBUBBLES

R. Imai, H. Nakagawa, T. Kanagawa, M. Watanabe and S. Fujikawa*
Division of Mechanical and Space Engineering,
Graduate School of Engineering, Hokkaido University, Sapporo, 060-8628, Japan

ABSTRACT. The resonant frequencies of lipid bubbles are measured from attenuation of ultrasound pulse propagating through the test cell filled with normal saline or lipid bubble solution. The attenuation spectrum has two dominant peaks in the frequency range of 0 through 15 MHz due to the energy absorption by lipid bubble resonant oscillations. The two peaks of attenuation spectrum are observed near the bands of 1.4 MHz and 11.5 MHz, respectively. The peaks of attenuation spectrum decrease with the decrease in the concentration of the lipid bubble solution. Furthermore, the strong attenuation is confirmed to be hardly affected by the length through the lipid bubbles. We conclude that the two peaks in the attenuation spectrum obtained are related to the effect of the existence of lipid bubbles.

Keywords: *Ultrasound, Lipid microbubble, Drug delivery system*

INTRODUCTION

Bubbles have been widely used in various fields, for instance, from marine engineering to medical engineering. One of the most characteristic features observed in the practical bubble application is a wide range of bubble diameter. Diameters of bubbles are of the order of millimeters when bubbles are used for the drag reduction of large vessel. On the other hand, they are of the order of nanometers when bubbles are used for clinical applications such as the contrast agents.

In the field of medical engineering, the application of bubbles to Drug Delivery System (DDS) has attracted great attention as the administration of next generation. DDS with bubbles of nanometer size is expected to be a noninvasive clinical treatment. Capsules of nanometer size, which contain exogenous gene such as anticancer drug, are administered in blood. These capsules are transported to target sites and impregnate in the disorder cells efficiently.

There exist bubbles wrapped in biomedical materials, i.e., lipid. The lipid bubbles are used as the transport carrier of DDS. However, dynamic properties of these lipid bubbles are not yet made clear. DDS with lipid bubbles uses actively the resonance of bubbles in order to increase the efficiency of gene injection in the disordered cell, because oscillations of lipid bubbles are easily excited with sufficiently small driving forces at resonant conditions.

In this study, acoustic characteristics of lipid bubbles are experimentally investigated in the vicinity of the resonance. The resonant frequencies of lipid bubbles are evaluated by measuring the attenuation of the propagating broadband ultrasound waves through the water containing lipid bubbles.

EXPERIMENTAL METHOD

Lipid bubble

* Corresponding author: Prof. S. Fujikawa
Phone: + (81)-11-706-6429, Fax: + (81)-11-706-6429
E-mail address: fujikawa@eng.hokudai.ac.jp

We use lipid bubbles in a liquid. A lipid bubble is composed of a kind of shell made of lipid layer, in which both gas and liquid are contained. The lipid bubble is made from a liposome. Figure 1 shows schematic diagrams of a lipid bubble. The liposome used in the present experiment is first made of lipid with DSPC (DiStearoyl Phosphatidyl Choline) and then modified by PEG (PolyEthlen Glycol Distearate). With the treatment, the liposome can exist stably in blood. The liposome becomes easily incorporated with ligand that is able to bind disease-related markers on bubble surfaces.

The liposome is produced by the reverse phase evaporation method. The inside of liposome produced by this method is liquid phase (Figure 1 (a)); hence liquid should be replaced by C_3F_8 (Perfluorocarbon) gas (Figure 1 (b)). The C_3F_8 gas is first injected into a glass receptacle containing a liposome solution, and then the receptacle is wobbled using an ultrasonic cleaner (Ultrasound cleaner 2510-J-DTH, Bransonic Co., Ltd.) until the solution in the receptacle becomes opaque. As shown in Figure 1 (b), it is supposed that replacement from the contained liquid to the gas within the liposome is attained by micelle formation inside the liposome [1]. The C_3F_8 gas enables lipid bubbles containing this gas to be used as an ultrasound contrast agent [2]. It is also necessary to equalize the size distribution of lipid bubbles by using the 20 kHz ultrasound probe. The lipid bubbles with larger diameters are assumed to be destroyed by this procedure. Figure 2 shows the distribution of lipid bubble diameter.

The solution containing lipid bubbles is diluted with the PBS (Phosphate Buffered Saline), and thus, solutions of different concentrations are obtained. The stock solution of lipid bubbles before diluted contains DSPC of 1 mg in its 1 ml. In this study, lipid bubble solutions with the concentration of 1000 ppm, 1333 ppm, 2000 ppm, and 4000 ppm are used. The experimental test cell which is the container made of the Polyvinylidene Chloride film (Saran Wrap, Asahi Kasei Co., Ltd.) is filled with lipid bubble solution. Ultrasound passes through this film.

Figure 3 shows the scanning electron micrograph of the liposome.

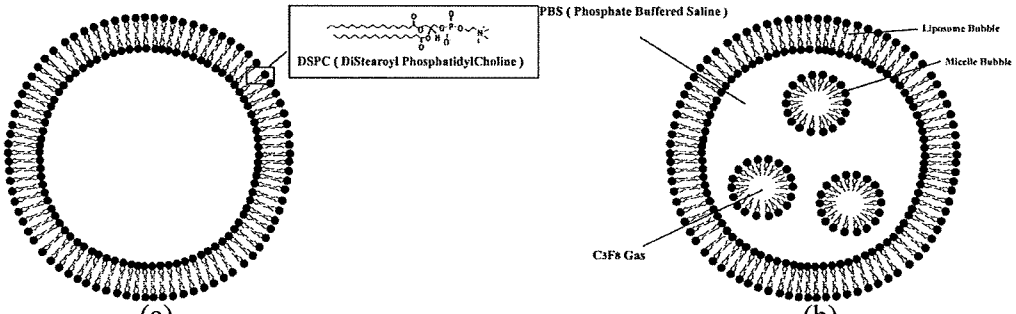

Figure 1. Schematic diagrams of a lipid bubble: (a) before gas replacement, (b) after gas replacement of liquid phase inside a liposome.

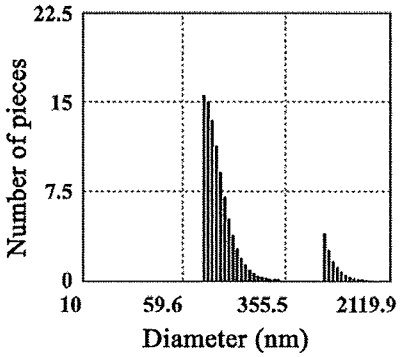

Figure 2. Distribution of lipid bubble diameter.

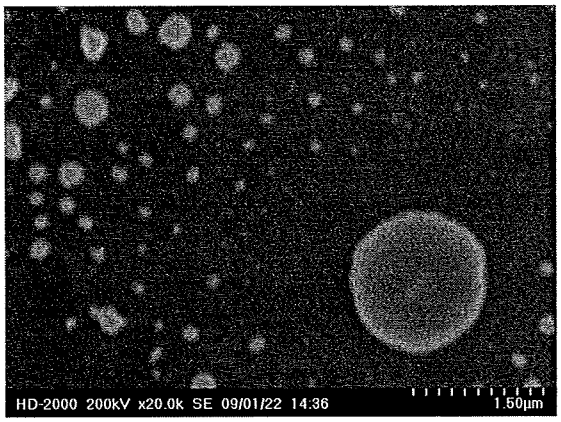

Figure 3. The scanning electron micrograph of the liposome.

Experimental apparatus and method

Experimental apparatus

Figure 4 shows the experimental apparatus, which is similar to that used by Hoff et al. [3]. This apparatus consists of a pulser/receiver, a coaxial cable relay for selecting transducers, four transducers (Panametrics Videoscan V306-SU, V382-SU, V326-SU and V312-SU), and a digital oscilloscope (LeCroy9410, LeCroy Co., Ltd.). The pulser/receiver and oscilloscope were connected to a PC.

Central frequencies of four types of broadband ultrasound transducers are 2.25MHz, 3.5MHz, 5.0MHz, and 10.0MHz, respectively. The four transducers are unfocused, 2.25 MHz with 13 mm aperture diameter, 3.5 MHz with 13 mm aperture, 5.0 MHz with 10 mm aperture, and 10.0 MHz with 6 mm aperture diameter. They are mounted in parallel in a water tank made of acrylic.

The test cell is filled with normal saline or the diluted lipid bubble solution. The lengths of the cell are 31.5 mm or 15.0 mm, and the distances from transducers to the experimental cell are 100 mm. The back wall of the water tank acts as an acoustic reflector, and is placed 150 mm from the transducer faces as shown in Figure 4. This acoustic reflector is made of steel.

Experimental method

The transducers are excited by the pulser which sends broadband ultrasound short pulses at 50 pulses per second. These pulses propagate through the experimental cell containing a lipid bubble solution separated from the ambient water by a very thin plastic film. These pulses are reflected at the back wall of the water tank, and then received by the transducer again. That is, the pulses pass through the cell twice; hence the total sound path lengths through the cells of 31.5 mm and 15.0 mm become 63.0 mm and 30.0 mm, respectively. The received pulses are amplified by the receiver and transferred to the oscilloscope. The oscilloscope is set to display only the reflection off the back wall of the chamber. The pulses are digitized in the oscilloscope at a sampling rate of 20 GS/s, and transferred to PC.

Signal processing of the received pulses is carried out using MATLAB software (The Math Works, Inc., Natick, MA). The power spectra are calculated by the Fast Fourier Transformation of received pulses in the cases of with and without lipid bubbles in the cell, respectively. Figure 5 shows an example of received pulses and their power spectra, without and with lipid bubbles in the cell with 31.5 mm in length. The attenuation spectra are calculated by the normalization, i.e., dividing the difference of power spectra both with and without lipid bubbles by the total sound path length through the cell, which is either 63.0 mm or 30.0 mm.

The evaluation ranges of broadband ultrasound transducers are from 1.4 to 3.0MHz, from 2.0 to 5.0MHz, from 3.0 to 8.0MHz, and from 6.0 to 14.0MHz, respectively, which correspond to their central frequencies 2.25MHz, 3.5MHz, 5.0MHz, and 10MHz. The overlaps of the curves obtained by different transducers assure the consistency of the experiment.